Design and Dynamic Modelling of 40 kW Solid Oxide Electrolysis System

Master Thesis

Miguel Azevedo Fialho de Oliveira Pinto

Aalborg University
Department of Energy

Department of Energy
Aalborg University
http://www.aau.dk

AALBORG UNIVERSITY
STUDENT REPORT

Title:
Design and Dynamic Modelling of 40 kW Solid Oxide Electrolysis System

Theme:
Master Thesis

Project Period:
Spring Semester 2025

Project Group:
HYTEC4-1014

Participant(s):
Miguel Pinto

Supervisor(s):
Xiaoti Cui

Number of Pages: 54

Date of Completion:
May 28th - 2025

Abstract:

Hydrogen production using electrochemical processes has gained significant interest, as a cleaner alternative to fossil fuel-based methods. High temperature electrolysis has been growing due to its enhanced thermodynamics and kinetics at elevated temperatures in comparison to low temperature electrolysis.
This thesis presents the design of a one-dimensional dynamic model of a 40 kW Solid Oxide Electrolyser Cell (SOEC) stack. The model consisting of electrochemical kinetics, mass, and energy balances, is employed to study the dynamic behaviour of the SOEC stack under step load changes, with spatial discretization applied to resolve temperature and composition profiles along the cell length. Balance-of-plant components such as heat exchangers and electric heaters are also included. The results demonstrate that the system achieves over 80 % efficiency over the simulation period. Transient behaviour under step load changes was stable, with temperature gradients remaining below 10 K/cm. The stack produced approximately 7 kg of hydrogen over a 10 hour simulation with a specific energy consumption close to 34 kWh/kg.
The model aims to demonstrate the SOEC's suitability for dynamic hydrogen production scenarios, supporting its integration in renewable-based energy systems.

The content of this report is freely available, but publication (with reference) may only be pursued due to agreement with the author.

Summary

The transition toward sustainable energy systems has increased the focus on hydrogen production through electrochemical processes, particularly as a clean alternative to conventional fossil fuel-based processes. Among these, Solid Oxide Electrolysis Cells (SOECs) have gained increasing attention due to their improved thermodynamic and kinetic performance at high operating temperatures, offering notable efficiencies and great integration potential with external heat sources. High temperature electrolysis facilitates the effective use of industrial waste heat and renewable electricity, making SOECs ideal candidates for dynamic, large-scale hydrogen production. Furthermore, these electrolysers provide remarkable fuel flexibility and possess the unique advantage of reversibility, operating either in electrolysis mode or as fuel cells depending on system requirements.

This thesis presents the development and simulation of a one-dimensional dynamic model of a 40 kW SOEC stack. The model incorporates electrochemical kinetics, mass and energy balances, and resolves temperature and species profiles along the cell length through spatial discretization. Additional system components such as heat exchangers and electric heaters are also integrated into the simulation framework. The entire model is implemented using MATLAB and Simulink, allowing the evaluation of both steady-state and transient system behaviour under step load changes.

Results show that the system achieves efficiencies over 80 % throughout a 10-hour simulation period. During dynamic operation, the stack demonstrates thermal stability, with temperature gradients remaining below the 10 K/cm limit, minimizing degradation risk. The model produces a total hydrogen output of approximately 7 kg and a specific energy consumption (SEC) of around 34 kWh/kg.

Despite simplifying assumptions such as adiabatic and isobaric conditions, the model demonstrates the technical feasibility of SOECs for integration into renewable-based hydrogen production systems. The results highlight the critical role of thermal management and control strategies in sustaining efficiency and limiting degradation during dynamic operation. Future work should focus on experimental validation and the inclusion of more detailed loss terms and start-up/shutdown dynamics.

Preface

The following thesis has been accomplished by the student Miguel Azevedo Fialho de Oliveira Pinto as part of the 4^{th} semester study plan of the master's degree at Aalborg University.

Reading Guide

The citations have been done using the Harvard method where citations will be shown as [Author(s), year]. The citations follow their references in the bibliography located at the end of the thesis. Chapters, sections, figures, tables and equations are labeled and these will also be references when mentioned in the text. The numbering of these labels is in chronological order and chapter-wise. Throughout the report, the symbols, abbreviations and subscripts can be found in the Nomenclature. The following software has been used in this project:

- Mathworks® MATLAB
- Mathworks® SIMULINK
- Microsoft Office
- Overleaf LaTeX®

Miguel Pinto
mpinto23@student.aau.dk

Signature

Aalborg University, May 27, 2025

Nomenclature

Standard SI-Units will be used

Symbol	Description	SI Unit
d_P	Average Pore diameter	[m]
$\dot{h}$	Specific Enthalpy	[J/kg]
l	Thickness	[m]
m	Mass	[kg]
$\dot{n}$	Molar flow rate	[mol/s]
p	Partial Pressure	[Pa]
t	Time	[s]
y	Molar fraction	[-]

Symbol	Description	SI Unit
A	Area	[m^2]
C_s	Stack Heat Capacity	[$J/kg \cdot K$]
C_P	Isobaric specific heat capacity	[W/m·K]
D	Diffusivity	[$kg/m^2 \cdot s$]
E_{act}	Activation energy	[J]
E_{rev}	Reversible cell voltage	[V]
E_{cell}	Cell voltage	[V]
E_{Nernst}	Cell voltage at non-standard conditions	[V]
F	Faraday Constant	[C/mol]
ΔG	Gibbs Free energy	[J]
ΔH	Enthalpy Change	[J/mol]
ΔS	Entropy Change	[J/mol·K]
I	Current	[A]
J	Current Density	[A/m^2]
J_0	Exchange Current Density	[A/m^2]
M	Molar weight	[g/mol]
M_s	Stack mass	[kg]
N	Number of Cells in the Stack / Species Production/-Consumption	[-] / [mol/s]
P	Pressure / Electrical power	[Pa] / [W]
$\dot{Q}$	Heat Transfer	[J]
R	Universal gas constant	[J/mol·K]
T	Temperature	[K]
U	Overall heat transfer coefficient	[$W/m^2 \cdot K$]
V	Volume / Diffusion Volume	[m^3]

Symbol	Description	SI Unit
γ	Pre-exponential factor	$[A/m^2]$
ε	Elecgtrode Porosity	[-]
ζ	Electrode tortuosity	[-]
$\eta_{act/ohm/conc}$	Overpotential activation/ ohmic/ concentration	[V]
ψ	Specific Thermal Conductivity	$[W/m \cdot K]$

Sub-/superscript	Description
x_{air}	Properties of air
$x_{an/ca/electrolyte}$	Anode/Cathode/Electrolyte
x_{cell}	Singular Cell from the Electrolyser Stack
x_{el}	Electrical aspect
x_{fuel}	fuel
$x_{in/out}$	Inlet/outlet condition
x_{sys}	Entire system
x_{s}	Plural
x_{stack}	Stack of Electrolyser
$x_{thermal}$	thermal aspect

Abbreviations

Abbreviation	Description
AEM	Anion Exchange Membrane
FC	Fuel Cell
GHG	Green House Gas
HHV	Higher Heating Value
HX	Heat Exchanger
LHV	Lower Heating Value
LMTD	Logarithmic Mean Temperature Difference
MIEC	Mixed Ionic-Electronic Conductors
ODE	Ordinary Differential Equation
PEM	Polymer/Proton Exchange Membrane
PtX	Power-to-X
PFSA	Perfluorosulfonic Acid
SOC	Solid Oxide Cell
SOEC	Solid Oxide Electrolyser Cell
SOFC	Solid Oxide Fuel Cell
TEG	Triethylene Glycol
TPB	Triple Phase Boundary
TRL	Technology Readiness Level
WGS	Water-Gas Shift
HWT	Hot Water Tank

Contents

List of Figures

List of Tables

Chapter 1

Introduction

There is a growing concern over climate change, environmental and animal habitat degradation, natural catastrophes, and human health. The great dependence on fossil fuels in the global energy system, rising year after year, has led to serious consequences. Resource depletion, air pollution, *greenhouse gas emissions* (GHG) are just a few of the negative effects of relying on fossil fuels. Over the last few years, the shift for sustainable energy solutions has gained significant awareness to mitigate these detrimental repercussions [Busch et al., 2023]. Green energy sources such as wind, solar, and hydro have received increasing attention. Among them, hydrogen has emerged as a promising energy carrier due to its wide versatility and potentially zero-carbon applications. The adoption of clean energy technologies is not only an environmental imperative but also a crucial economic and geopolitical strategy to achieve energy independence [International Energy Agency, 2024].

1.1 Green Energy Transition

The European Commission, on the 14th of July 2021, presented the "Fit for 55" plan, which refers to the EU's target of reducing net GHG emissions by at least 55 % by 2030 compared to the 1990 levels [EuropeanCommission, 2021]. The European Green Deal aims to align with the objectives outlined in the Paris Agreement, which seeks to limit the global average temperature rise to well below 2°C above pre-industrial levels, while striving to further restrict the increase to 1.5°C [Alsagr et al., 2024].
However, the expansion of renewable energy sources as a means to achieve the European Commission goal introduces several challenges, including the use of critical raw materials, waste generation, and inherent energy fluctuations. The latter require effective storage solutions to ensure a stable energy supply. One well-established technology to address this affair is the *Power-to-X* (PtX), a technology that converts excess renewable energy into storable and transportable energy carriers such as ammonia, methanol, or hydrogen.

1.2 Fuel Cells and Electrolyzers

Fuel cells (FCs) and Electrolyzers play a critical role in the hydrogen economy, enabling the production and utilisation of hydrogen as a clean energy source. FCs represent an innovative technology in energy production as an alternative to traditional fossil fuel combustion. Developed in the 19th century, FCs have undergone significant advancements and improvement, and are now considered a viable option for green energy production. FCs operate by converting chemical energy into electric energy through an electrochemical reaction, producing only water and heat as byproducts. This makes them ideal for applications in transportation, stationary power generation, and portable energy solutions.

Electrolyzers, on the other hand, produce hydrogen by splitting water into hydrogen and oxygen using electricity. When powered by renewable energy, electrolyzers provide a sustainable method of generating green hydrogen, which can be stored, transported, and utilized in various sectors.
Electrolyzers serve as key PtX devices addressing the challenge of energy fluctuations by allowing excess renewable energy to be utilized effectively rather than remaining unused. Various electrolyser types are presented in the table below [Rathee, 2023]:

Type	**AEM**	**Alkaline**	**PEM**	**SOEC**
Electrolyte	Anion exchange ionomer	Aqueous potassium hydroxide	PFSA membranes	Yttria Stabilized Zirconia (YSZ)
Anode	Nickel, Ferrous, Cobalt oxides	Nickel, Nickel-Cobalt alloys	Ruthenium oxide, Iridium oxide	YSZ
Cathode	Nickel and Nickel alloys	Nickel, Nickel-Molybdenum alloy	Platinum, Platinum-Palladium alloy	Nickel/YSZ
Operating Pressure (bar)	1–30	30	70	1–25
Operating Temperature (ºC)	50–60	60–80	50–80	500–900
Stack Lifetime (h)	–	60–100k	20–60k	<10k
TRL	5–6	9	9	9

Table 1.1: Comparison of Electrolyzers

As shown in Table 1.1, different electrolyser technologies exhibit distinct characteristics. These are in electrolyte composition, operating conditions, stack lifetime, and *technological readiness level* (TRL). Each type offers specific advantages and limitations depending on its application, efficiency, and cost considerations. Among these, alkaline, PEM, and SOEC electrolysers are the most commercially established, with the latter holding high-temperature operations and improved efficiency. Meanwhile, AEM electrolyzers are emerging as a potential alternative due to their cost-effectiveness and operational flexibility.

The integration of FCs and electrolyzers into energy systems is a crucial step towards carbon-neutrality. Moreover, the ability to store and transport hydrogen enhances its role in fostering a circular and sustainable economy. As advancements in hydrogen infrastructure grow through ongoing research and investment, FCs and electrolyzers will become integral to the global energy transition, strengthening resilience in an increasingly renewable-dependent world.

Chapter 2

Problem Statement

In the quest for sustainable energy solutions, *solid oxide electrolysis cells* (SOECs) have emerged as a versatile and promising technology due to their reversible operation for hydrogen and electrical energy production, potential for combined heat and power applications, and integration with diverse energy sources or industries. The accrescent transition toward carbon-neutral energy solutions has accelerated the development of efficient, durable and reliable SOEC systems, making them essential for achieving long-term sustainability goals. This thesis focuses on the design and modelling of a 40 kW SOEC system, analysing its performance under steady state and dynamic conditions. The study involves a detailed analysis of the electrolysis process, examining the operating conditions, reaction kinetics, and thermal management strategies that influence system efficiency and longevity. Beyond the SOEC stack, balance of plants components such as heat exchangers, and electrical heaters are also included, forming a comprehensive setup designed to address the following research questions:

- What is the overall system efficiency under steady state and dynamic conditions?
- What are the key parameters influencing the production of hydrogen on a SOEC?
- How does the SOEC system respond to transient load changes, and what are the implications for system stability and control?

2.1 Methodology

To answer the research questions, MATLAB and Simulink models are developed to simulate the operation of the SOEC system under steady-state and dynamic conditions. These include the modelling of all the essential components required for system operation. In the absence of experimental data, the obtained results are compared with existing literature to ensure accuracy and consistency.

Chapter 3

Modelling

The scope of this chapter is to illustrate how the modelling of the components is performed and to introduce the operation of SOECs, and explore key factors influencing their performance. In addition to the fundamental working principles, this chapter discusses the impact of material composition, thermodynamics, and electrochemical behaviour. Furthermore, it addresses efficiency considerations, degradation mechanisms, and potential advancements in SOECs technology, providing a comprehensive understanding of their role in energy conversion and storage.

3.1 Working Principle

SOECs were first conceptualized in the late 19^{th} century when Nernst discovered solid electrodes which laid the foundation for high temperature ionic conduction. Later, it led to the development of *Solid Oxide Fuel Cells* (SOFCs), and, subsquently, SOECs [Funke, 2013]. There are two main structural configurations, planar and tubular. The planar structure featuring an easier manufacturing and high performance, while the tubular offering an enhanced mechanical strength and gas-tightness [Sitte and Merkle, 2023].

The SOECs operate at elevated temperatures (500-1000 ºC) offering thermodynamic benefits for hydrogen production [Laguna-Bercero, 2023]. To withstand these high temperatures, SOECSs are composed of special materials resistant to thermal degradation, high ionic and electronic conductivity, and selectivity. SOECs' electrolyte are typically made of *yttria-stabilized zirconia* (YSZ) or other oxide-ion-conducting ceramics, enabling the transport of oxygen ions O^{2-} at high temperatures. During the electrolysis reaction, electricity is applied to convert water (H_2O) into hydrogen (H_2) and oxygen (O_2) contrasted in the following reaction [O'Hayre et al., 2016]:

$$H_2O + \text{Electricity} \rightarrow H_2 + \frac{1}{2}O_2 \tag{3.1}$$

The primary electrochemical reaction (3.1) takes place at the electrolyzer's electrodes, specifically at the cathode and anode [Menon et al., 2014].

$$\text{Cathode: } H_2O + 2\,e^- \rightarrow H_2 + {O_2}^- \tag{3.2}$$

$$\text{Anode: } {O_2}^- \rightarrow \frac{1}{2}O_2 + 2\,e^- \tag{3.3}$$

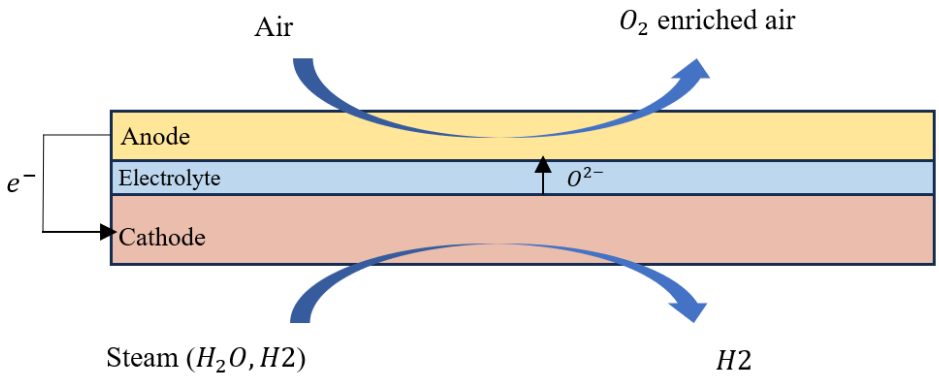

Figure 3.1: SOEC cell sketch

An unique characteristic of SOECs is their reversibility. Unlike conventional electrolyzers, SOECs can operate in both electrolysis and FC modes. This dual functionality allows the production of H_2 when excess electricity is available and, conversely, generate electricity from H_2 when needed. As illustrated in Equations (3.2) and (3.3), the operating mode of *Solid Oxide Cells* (SOCs) relies on the electrochemical reactions happening between oxidizing and reducing species. If operated in FC mode, H_2O and electricity are produced through the oxidation of the fuel and reduction of O_2. As for electrolysis mode, the reactions inverse under electrical energy.

3.2 Electrochemical Kinetics

The theoretical energy required to split H_2O into H_2 and O_2, ΔH is [O'Hayre et al., 2016]:

$$\Delta H = \Delta G + T\Delta S \tag{3.4}$$

where ΔG represents the Gibbs free energy, which is the minimum energy required for a process to occur at constant pressure and temperature, T is temperature, and ΔS is the entropy change.

The reversible voltage E_{rev} representing the minimum voltage required between the cathode and the anode for the electrolysis to happen can be expressed as:

$$E_{rev} = -\frac{\Delta G}{zF} \tag{3.5}$$

where z denotes the number of electrons transferred in the reaction and F is the Faraday constant.

If the thermal energy demand is provided by electric energy, the thermoneutral voltage E_{th} is the actual minimum voltage for the H_2O dissociation which can be obtained from the following [Buttler et al., 2015]:

$$E_{th} = \frac{\Delta H}{zF} \tag{3.6}$$

The equilibrium voltage required by a SOEC at non-standard conditions, taking into account species concentration, partial pressures, etc., is known as the Nernst Equation, E_{Nernst}, which can then be expressed as [Menon et al., 2014]:

$$E_{Nernst} = E_{rev} + \frac{RT}{zF} ln \left(\frac{p_{H_{2_c}} p_{O_{2_a}}^{\frac{1}{2}}}{p_{H_2O_c}} \right) \tag{3.7}$$

where R is the universal gas constant and p_i represents the partial pressures of H_2, H_2O at the cathode, and O_2 at the anode.

In practical, the charge transfer chemistry takes place at the *triple phase boundaries* (TPB), which are the interfaces where electrocatalyst, electrolyte and gas-phase meet, and the reaction needs to overcome deviations between the electrode potential and the equilibrium potential caused by various irreversible losses and this phenomenon is referred to as polarization. The operating cell voltage is then calculated after taking into account all the irreversibilities that occur during the operation [Wu et al., 2024].

$$E_{cell} = E_{Nernst} + \eta_{act} + + \eta_{ohm} + + \eta_{con} \tag{3.8}$$

where η_{act}, η_{ohm} and η_{con} represent the activation, ohmic and concentration overpotentials respectively.
For the activation overpotential, or polarisation, since it is caused by the electrode kinetics and represent the overpotential required for the electrochemical reaction, it can be calculates for both electrodes, i.e., the cathode and anode as [Ni et al., 2007]:

$$\eta_{act} = \frac{RT}{F} sinh^{-1}(\frac{J}{2J_{0,i}}) \tag{3.9}$$

where J represents the current density, $J_{0,i}$ the exchange current density which indicates how readily the electrode is to proceed with the reaction, and i for cathode and anode. According to [Ni et al., 2007], the exchange current density, $J_{0,i}$, can be expressed as:

$$J_{0,i} = \gamma_i \; exp(-\frac{E_{act,i}}{RT}) \tag{3.10}$$

where γ_i denotes the pre-exponential factors of the anode and cathode and $E_{act,i}$ the activation energy.

The calculation of the ohmic overpotential is relatively straightforward, as the electrical connecting plates and electrodes typically possess significantly higher electrical conductivity than the electrolyte. Consequently, their contribution to the overall ohmic overpotential can be considered negligible. Therefore, it can be found through [Ni et al., 2007]:

$$\eta_{ohmic} = 2.99 \times 10^{-5} \; J \; l_{\text{electrolyte}} \; exp(\frac{10300}{T}) \tag{3.11}$$

with $l_{electrolyte}$ standing for the electrolyte thickness.

The concentration overpotential, η_{con}, arise due to mass transport limitations of reactants and products at the TPB. According to [Mohebali Nejadian et al., 2023], the concentration overpotentials can be calculated as follows:

$$\eta_{\text{concentration, an}} = \frac{R \times T}{zF} \times \ln\left(\left(1 + \frac{J \times R \times T \times l_{\text{an}}}{4F \times D_{\text{effective,an}} \times p_{O_2}}\right)^{0.5}\right) \tag{3.12}$$

$$\eta_{\text{concentration, cat}} = \frac{R \times T}{zF} \times \ln\left(\frac{1 + \frac{J \times R \times T \times l_{\text{ca}}}{2F \times D_{\text{effective ca}} \times p_{H_2}}}{1 - \frac{J \times R \times T \times l_{\text{ca}}}{2F \times D_{\text{effective ca}} \times p_{H_2O}}}\right) \tag{3.13}$$

where l_{an} and l_{ca} stand for the anode and cathode electrode's thickness and $D_{\text{effective}}$ for its effective diffusion.

The electrolysis process is significantly influenced by diffusion mechanisms, as they play a fundamental role in the transport of gaseous and ionic species within electrochemical systems, directly impacting overall performance. Two primary types of diffusion contribute to this process: molecular diffusion and Knudsen diffusion. The combined effect of these mechanisms determines the effective diffusion coefficient, which governs the mass transport efficiency within the system.
The molecular diffusion coefficient is described by Fuller's correlation and depends on the species' binary diffusion volume. The Knudsen diffusion is governed by the kinetic theory of gases and is dependent on the average pore radius. Equations (3.14) and (3.15) describe the necessary calculations to find the diffusion values to use in Equations (3.12) and (3.13) [Mohebali Nejadian et al., 2023] [Perna et al., 2018]:

$$\frac{1}{D_{\text{effective, an}}} = \frac{\varepsilon}{\xi} \times \left(\frac{1}{D_{\,\text{O}_2-N_2}} + \frac{1}{D_{\,\text{Kun O}_2}}\right) \tag{3.14}$$

$$\frac{1}{D_{\text{effective, ca}}} = \frac{\varepsilon}{\xi} \times \left(\frac{1}{D_{\text{H}_2-H_2O}} + \frac{1}{D_{\,\text{Kun H}_2O}}\right) \tag{3.15}$$

$$D_{\,\text{H}_2-H_2O} = 0.00143 \times \frac{T^{1.75}}{P \times \left(\frac{2}{M_{H_2}^{-1}+M_{H_2O}^{-1}}\right)^{0.5} \times \left(V_{\text{H}_2}^{\frac{1}{3}} + V_{\text{H}_2O}^{\frac{1}{3}}\right)^2} \tag{3.16}$$

$$D_{\text{O}_2-N_2} = 0.00143 \times \frac{T^{1.75}}{P \times \left(\frac{2}{M_{O_2}^{-1}+M_{N_2}^{-1}}\right)^{0.5} \times \left(V_{\text{O}_2}^{\frac{1}{3}} + V_{\text{N}_2}^{\frac{1}{3}}\right)^2} \tag{3.17}$$

$$D_{\,\text{Kun H}_2O} = \left(\frac{d_p}{3} \times \left(8 \times R \times \frac{T}{\pi \times M_{\text{H}_2O}}\right)^{0.5}\right) \tag{3.18}$$

$$D_{\,\text{Kun O}_2} = \left(\frac{d_p}{3} \times \left(8 \times R \times \frac{T}{\pi \times M_{\text{O}_2}}\right)^{0.5}\right) \tag{3.19}$$

with ε and ξ standing for the electrode porosity and tortuosity, respectively, V_i for the Fuller's binary diffusion volumes of the corresponding species, and M_i for the species

molar weight.
The proper evaluation of diffusion mechanisms is essential in optimizing electrode design and material selection for SOECs. Factors including pore size, electrode thickness, gas composition, and operating temperature all influence the diffusion characteristics. An insufficient diffusion rate can lead to concentration polarization, reducing overall cell efficiency. By considering both molecular and Knudsen diffusion effects, the transport limitations of reactants and products in porous media can be minimized.

Gas species	Diffusion volume
H_2	6.12
H_2O	13.1
N_2	18.5
O_2	16.3

Table 3.1: Diffusion volumes for different gas species [Hauck et al., 2017].

Considering an isothermal operation, there are several possibilities regarding the cell or stack voltage output:

- if $E < E_{rev}$ the reaction can not occur.
- if $E_{rev} < E < E_{th}$ the reaction is possible by adding heat in order to maintain isothermal conditions
- if $E = E_{th}$ the heat produced and required by the cell/stack are equal and electrolysis occurs without the need to add nor extract thermal energy.
- if $E > E_{th}$ electrolysis is possible under isothermal conditions if the heat produced by the cell/stack is dissipated.

Ultimately, the thermoneutral voltage determines whether the SOEC operates in endothermic or exothermic mode, each with its own advantages and drawbacks. However, SOECs are typically operated at thermoneutral voltage to simplify the system [Buttler et al., 2015]. To calculate the amount of H_2 produced during the electrolysis process, which is linearly inverse to the H_2O consumed and dependent on the current, it is possible to find through [Lay-Grindler et al., 2013]:

$$\dot{n}_{\mathrm{H_2}} = -\dot{n}_{\mathrm{H_2O}} = \frac{I}{2F} \tag{3.20}$$

And for O_2:

$$\dot{n}_{\mathrm{O_2}} = \frac{I}{4F} \tag{3.21}$$

Since not all of the H_2O introduced in the feed gas is converted to H_2, the steam utilisation factor, U_f, is defined to explicitly quantify the fraction of H_2O that undergoes conversion during the electrolysis process:

$$U_f = \frac{\dot{n}_{\mathrm{H_2O},consumed}}{\dot{n}_{\mathrm{H_2O},in}} = \frac{\frac{I}{2F}}{yH_2O \times \dot{n}_{\mathrm{steam}}} \tag{3.22}$$

U_f range is between 0 and 1, each end of the spectrum offering its own advantages and disadvantages. Operating at a high steam conversion rate improves efficiency by maximizing H_2 production per unit of steam, reducing the need for excess steam input [Cai et al., 2010]. However, it can also lead to mass transport limitations and potential thermal instability, which may impact cell durability. On the other hand, working with a lower U_f ensures better temperature uniformity and reduces degradation risks but comes at the cost of increased energy consumption and additional requirements for steam recycling. Therefore, selecting the optimal steam utilization factor requires balancing efficiency, system longevity, and operational complexity to achieve the best performance in SOEC applications.

The electrical efficiency of a SOEC is determined by considering the amount of H_2 produced during electrolysis in relation to the energy input. It can be calculated using the following expression:

$$\eta_{SOEC} = \frac{\dot{n}_{\mathrm{H_2}} \times LHV_{H_2}}{P_{el}} \tag{3.23}$$

where LHV_{H_2} stands for the lower heating value of hydrogen and P_{el} is the electrical power input.

3.3 Mass and Energy Balance

The electrochemical model is directly affected by temperature and species composition. Since these vary with time under dynamic operations, it is essential to correctly define how they progress. The governing equations are defined along a one-dimensional spatial axis and discretized into 10 segments to capture the spatial evolution of temperature and species concentrations.

For the thermal analysis it is important to underline the following assumptions:

- Heat losses are neglected, assuming an exceptional insulation of the system.
- A semi-lumped thermal model is adopted: the temperature is assumed to vary along the length of the cell, but is considered uniform across the different components (electrodes, electrolyte, interconnects, etc.) at each segment.
- No active or passive cooling is implemented.
- The streams are considered to be ideal gas.

For each segment of the discretized cell length, the mass and momentum governing equations are [Wang et al., 2020]:

$$\frac{dM_i}{dt} = \dot{n}_{in,i} \pm n_{react,i} - \dot{n}_{out,i} \tag{3.24}$$

$$n_{react,i} = \frac{JNA_{cell}}{zF} \tag{3.25}$$

$$P_{\text{in}} = \sum_{i=1}^{4} P_{\text{in},i} \tag{3.26}$$

$$\dot{n}_{\text{out,cathode}} = \sum_{i=1}^{2} \dot{n}_{\text{out},i} \tag{3.27}$$

$$\dot{n}_{\text{out,anode}} = \sum_{i=1}^{2} \dot{n}_{\text{out},i} \tag{3.28}$$

with i denoting the type of species (H_2, H_2O, O_2 and N_2), M_i the molar quantity of the species, $\dot{n}_{in}$ and $\dot{n}_{in}$ are the molar flow rates into and out of the segment, $\pm$ is positive for species produced and negative for species consumed, and $\dot{n}_{react}$ is the molar flow rate produced or consumed by the electrochemical reaction. P_{in} denotes the stream pressure.

The energy conservation equation, shown in Equation (3.29), includes various terms representing the energy entering and leaving the system. The positive terms correspond to energy inputs, which include the enthalpy changes of the inlet streams, namely, the cathode and anode flows, as well as the electric power supplied to the system. On the other hand, the negative terms account for the energy leaving the system, which denotes the enthalpy changes of the outlet streams and the heat required for the electrolysis process.

$$C_s M_s \frac{dT_c}{dt} = \dot{n}_{\text{in},i}\dot{h}_{\text{in},i} - \dot{n}_{\text{out},i}\dot{h}_{\text{out},i} \pm \cdot\dot{n}_{\text{chem},i}\dot{h}_{\text{out},i} + P_{el} - \dot{Q}_{rxn} \tag{3.29}$$

where C_s denotes the stack heat capacity, M_s the stack mass, and $\dot{h}$ the specific enthalpy. $\dot{Q}_{rxn}$ is the heat demand for the electrolysis process which can be expressed as [Huo et al., 2021].

$$Q_{rxn} = \frac{I}{2F} N\, LHV_{H_2} \tag{3.30}$$

3.4 SOEC from Elcogen

The SOEC parameters employed in this study are based on the Cell Stack "Elcogen E-3000" provided by the company Dynelectro. Most of the SOEC parameters used in this study are sourced from Elcogen website, with the exception of experimental parameters, which are detailed later.

3.4.1 SOEC Geometry

The development of SOECs has significantly advanced in recent years due to the increasing focus on green energy solutions to achieve carbon neutrality. The geometry and materials used in these stacks vary among manufacturers. SOEC stacks can have either a tubular or planar geometry, with the latter being the most commonly used [Sitte and Merkle, 2023]. Each geometry has distinct advantages and drawbacks, influencing the choice of design. Planar cells offer higher power densities, are easier to stack in series for industrial applications, and benefit from a well-established manufacturing process. However, they are also more prone to thermal stresses, which can lead to cracking, and they require exceptional sealing to ensure long-term operation. Tubular cells, on the other hand, provide greater mechanical strength and higher stability compared to planar cells. However, they have

lower power densities, and are more complex and costly to manufacture.

The cell stack provided by Dynelectro and used in this project, adopts a planar geometry.

3.4.2 SOEC Materials

SOECS typically consist of a 3 layer solid structure, composed of the air electrode/porous anode, electrolyte, and fuel electrode/porous cathode, and an interconnect plate. Each layer serves a different purpose for the stack operation, leading to diverse material composition.

Electrolyte

The electrolyte may be composed of different materials, depending on their ionic conductivity. The electrolyte is the core part of the SOEC stack and it is responsible for the ions transportation between the cathode and anode electrodes. Depending on the type of the SOEC stack, the electrolyte can be either an O_2 ionic conductor or a proton conductor. In order to effectively conduct the electrochemical reactions, the electrolyte must fulfil certain a set of conditions, such as [Laguna-Bercero, 2023]:

- High ionic conductivity.
- Gas tightness.
- Chemical compatibility with electrodes materials.
- Thermo-mechanical stability.
- Long term stability to ensure low degradation.
- Low cost of raw materials and manufacturing.

Despite the extensive study and proposal of numerous ionic conductive materials, Zirconium oxide (ZrO_2) doped with 3 % or 8 % mol of yttria (Y_2O_3) is currently the reference material for the electrolyte due to its chemical stability, abundance, low cost, and exceptional ionic conductivity. Hence, 3YSZ and 8YSZ are considered a state-of-the-art electrolyte material.

The electrolyte used in the present study is YSZ, however, due to confidentiality, specific doping materials and concentrations remain undisclosed.

Anode Electrode

Air electrodes in SOECs must fulfil a number of requisites to ensure optimal performance and long-term stability. An important factor to consider is the electrode's ability to efficiently release the O_2 that migrates through the electrolyte. Mixed ionic–electronic conductors (MIECs) are recommended since they offer high electrocatalytic activity and conductivity for the O_2 ions, products from the reduction of H_2O vapour, to produce O_2. Strontium-doped lanthanum manganite $(La_{1-x}Sr_xMnO_{3-\delta})(LSM)$, was used for several

years as a reference material for the anode electrode. However, due to recent advancements, LSM has been replaced by Lanthanum Strontium Cobalt Oxide $(La_{1-x}Sr_xCoO_3)(LSC)$, and lanthanum strontium cobalt ferrite $(La_{1-x}Sr_xCo_{1-y}Fe_yO_{3-\delta})(LSCF)$, due to their enhanced ionic-electronic conductivity [Smolinka and Garche, 2022].

In spite of their higher performance, it was observed that these materials reacted with YSZ. Therefore, a barrier layer based on gadolinia-doped ceria, $(Ce_{0.9}Gd_{0.1}O_{1.95})$(CGO), is inserted between the electrode and the electrolyte to prevent this reaction from occurring.

The anode electrode material used in this study is composed of LSC [Elcogen, 2025].

Fuel Electrode

Cathode or fuel electrodes used in SOECs are an essential component to take into consideration as it is where the electrochemical reduction of H_2O vapour into H_2 and O_2 ions takes place. Along with the other layers of the stack, the fuel electrode must provide an efficient ionic-electronic conductivity and a high electrocatalytic activity to facilitate the diffusion of electrons and oxide ions [Zhang et al., 2020]. Additionally, it must be compatible with the other components which is adjacent to, mechanically and chemically stable to ensure long-term operation and efficient reduction reactions, sufficiently porous to supply gas reactions and products removal, and cost-effective.
Nickel (Ni) is an outstanding material for the H_2O vapour reduction because of its high electrocatalytic activity. However, since it does not naturally conduct oxide ions, it is usually mixed with oxide ions conductive materials such as those used in the electrolyte. This addition enhances the electrode–electrolyte thermo-mechanical compatibility and prevents Ni agglomeration. Several materials have been extensively studied for use in the fuel electrode but none possess the combined properties of Ni-based cermets. Therefore, the state-of-the-art material employed in the cathode electrode consists of a cermet composed of approximately 40 vol% Ni and 60 vol% of the electrolyte material [Smolinka and Garche, 2022].

The Dynelectro stack cathode electrode material, and used in this study, is composed of NiO-YSZ [Elcogen, 2025].

Stack Properties

The following table illustrates the stack characteristics and the values chosen for the present project.

Parameter	Value	Reference
Operating temperature, T (K)	973.15	[-]
Operating pressure, P (bar)	1.0	[-]
Pre-exponential factor for anode exchange current density, γ_a (Am^{-2})	2.051×10^9	[[Ni et al., 2007]]
Pre-exponential factor for cathode exchange current density, γ_c (Am^{-2})	1.344×10^{10}	[[Ni et al., 2007]]
Activation energy for anode, $E_{act,a}$ ($Jmol^{-1}$)	1.2×10^5	[[Ni et al., 2007]]
Activation energy for cathode, $E_{act,c}$ ($Jmol^{-1}$)	1.0×10^5	[[Ni et al., 2007]]
Electrode porosity, ε	0.4	[[Buttler et al., 2015]]
Electrode tortuosity, ξ	5	[[Buttler et al., 2015]]
Average pore diameter, d_p (μm)	1	[[Buttler et al., 2015]]
Anode-supported electrolyzer		
Electrolyte thickness, $l_{electrolyte}$ (μm)	5	[[Elcogen, 2025]]
Cathode thickness, l_{ca} (μm)	15	[[Elcogen, 2025]]
Anode thickness, l_{an} (μm)	300	[[Elcogen, 2025]]
Cell Parameters		
Number of stacks, (-)	4	[-]
Number of cells per stack, (-)	119	[[Elcogen, 2025]]
Active cell area, A_{cell} (cm^{-2})	121	[[Elcogen, 2025]]
Mass of the stack, M_s (kg)	33	[[Elcogen, 2025]]
Average specific heat capacity of the stack, C_s (J kg^{-1} K^{-1})	500	[[Elcogen, 2025]]
Input Parameters		
Feed, (kg/h)	20	[-]
$x_{H_2,in}$, (-)	0.5	[-]
$x_{H_2O,in}$, (-)	0.5	[-]
Air Supply, (kg/h)	25	[-]
$x_{O_2,in}$, (-)	0.21	[-]
$x_{N_2,in}$, (-)	0.79	[-]

Table 3.2: SOEC parameters used in modelling analysis

A common practice in SOECs is to introduce a H_2 fraction of approximately 5% to 25% into the feed steam. This addition serves as a protective measure to prevent the oxidation of Ni in the electrode, which could otherwise compromise the cell's performance and longevity [Smolinka and Garche, 2022]. The presence of H_2 helps maintain a reducing environment,

mitigating the risk of Ni oxidation, which can lead to electrode deterioration and increased resistive losses. Additionally, this H_2 fraction can influence the electrochemical reactions occurring at the electrode, potentially enhancing overall system efficiency and operational reliability.

Due to confidentiality concerns, the experimental values used for electrochemical kinetics modelling were sourced from existing literature rather than the Dynelectro database. However, to assess the certainty and reliability of the obtained results, these will be discussed later in Section 4.

3.5 Heat Exchangers

In the present study, the Heat Exchangers (HX) are assumed to be adiabatic and heat losses are neglected, including conduction, convection and radiation. Energy balance equations are based on counter-current flow and 0D objects [Sitte and Merkle, 2023].

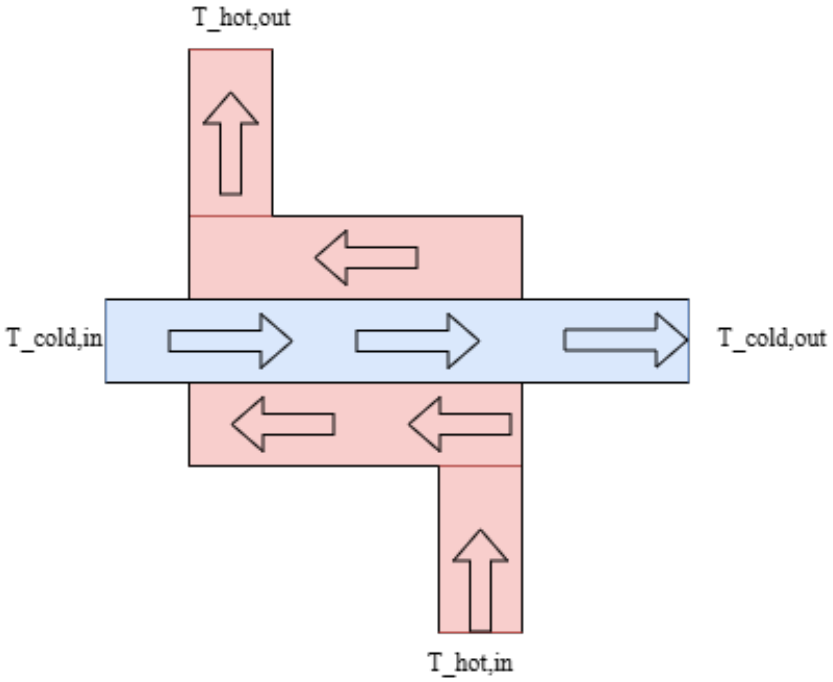

Figure 3.2: Counter-current HX schematic

3.5.1 Fuel Side HX

The fuel stream is composed of a H_2O and H_2 mixture as illustrated in Table 3.2. This mixture is assumed to be at constant temperature before entering the HX but it needs to be heated to match the working temperature of the SOEC. This heat exchange is highly benefic since it preheats the feed stream before going into the SOEC but it also cools down the outlet stream of the stack. This step is vital since the H_2 rich gas must be cooled down to further condense the H_2O present in the mixture and extract the H_2.

There are two main methods for HX design and analysis, the *Logarithmic Mean Temperature Difference* (LMTD) method, and the *Number of Transfer Units* (NTU) effectiveness method [Lienhard and Lienhard, 2024]. The LMTD method is adopted in this project. The cold inlet stream enters the HX at 423.15 K while the outlet temperature is initially unknown. To calculate it, a pinch point temperature difference of 40 K between the cold and hot stream is included [Petipas et al., 2013]. However, the outlet temperature does not reach the high operating temperature of the SOEC, requiring the use of an electric heater, which is approached later on. As for the hot stream, it varies between 953.15 K and 983.15 K depending on the transient system behaviour and it leaves the HX between 610 K and 630 K.
The modelling of the HX is assessed taking into account the energy balance equations for both streams. Since the cold stream is already in vapour phase, the enthalpy of vaporisation (latent heat) is not considered. The heat transfer process is modelled as a counterflow HX, where the heat transfer rate is determined based on the LMTD method. The energy balance equations for both streams can be expressed as follows [Sitte and Merkle, 2023]:

$$\dot{Q}_{\mathrm{HX}} = UA \cdot \Delta T_{\mathrm{mean}} = \dot{n} \cdot \mathrm{C_P} \cdot \Delta T \tag{3.31}$$

where UA stands for the the overall heat transfer coefficient multiplied by the heat exchange surface area and T_{mean} the logarithmic mean temperature difference which can be found by:

$$\Delta T_{\mathrm{mean}} = \mathrm{LMTD} \equiv \frac{\Delta T_a - \Delta T_b}{\ln\left(\frac{\Delta T_a}{\Delta T_b}\right)} \tag{3.32}$$

The cold stream outlet temperature is calculated the pinch constraint:

$$T_{\mathrm{c,out}} = T_{h,in} - 40 \tag{3.33}$$

where 40 is the pinch point temperature difference.
As for the hot stream outlet temperature, using Equation (3.31):

$$T_{\mathrm{h,out}} = T_{h,in} - \frac{\dot{Q}}{\dot{n}_h \cdot \mathrm{C_{P,h}}} \tag{3.34}$$

After the outlet stream temperatures are found, it is possible to calculate the LMTD and consequently the UA value using Equation 3.31.

3.5.2 Air Side HX

The air stream entering the SOEC must match the working temperature of the stack to prevent degradation and minimize temperature gradients that could lead to thermal stress. To achieve this, a second HX is used to preheat the air before entering the stack, which is modelled similarly to the fuel-side HX, with the main difference being the composition of the streams. The hot stream consists of exhaust gases from the SOEC anode, while the cold stream is air supplied by a blower at 293.15 K. However, the outlet temperature of the cold stream is insufficient to maintain the stack temperature, therefore an electric heater is placed before the stack to ensure the operating temperature, just as in the cathode side.

3.6 Electric Heaters

As explained previously, the HXs alone are insufficient to raise the steam mixture to the SOEC working temperature. Therefore, electric heaters are placed between the HXs and the SOEC to provide that additional heat required. The modelling of these components is relatively simple as only the electrical input is the calculated parameter:

$$\dot{Q}_{heater} = \dot{n}\ C_{\mathrm{P}} \Delta T \tag{3.35}$$

where m is either the steam mixture or air flow rate depending on the HX, and ΔT is the temperature difference between the SOEC working temperature and the HXs outlet temperature.

3.7 Balance of Plant

The system is composed of the set of components listed above. The modelling of the entire system is performed in SIMULINK due to the several connections between elements. These include the exhaust temperature and molar flow rates of the SOEC to both the Fuel HX and Air HX, feed stream into the HX, then the electric heater and later the SOEC, etc. It is important to ensure that despite the multiple elements, the model runs as just one. The efficiency of the system, or in other words, the *Balance of Plant* (BoP), is calculated taking into account the amount of energy in H_2 to the total electrical power input. It is similar to Equation (3.23) but it consider additional terms.

$$\eta_{Sys} = \frac{\dot{n}_{\mathrm{H_2}} \times LHV_{H_2}}{P_{SOEC} + P_{El\ Heaters}} \tag{3.36}$$

Chapter 4

Results

The following section aims to present and analyse the results obtained from the simulation performed in MATLAB and Simulink. The results provide a comprehensive assessment of the system's performance under the given operating conditions shown in Section 3.4. Key performance indicators such as system behaviour, stack and system efficiency, exhaust gas composition, electrical power output, and others are evaluated to gain insights into the operational characteristics of the SOEC system.

4.1 Steady State Performance

The SOEC stack has firstly been modelled in steady-state conditions to evaluate its performance and the outputs obtained. In a steady-state operation, parameters such as temperature, pressure, current, etc., do not change over time, therefore they remain constant throughout the operation. The pressure drop is assumed to be negligible at a working pressure of 1 bar [Udagawa et al., 2007].

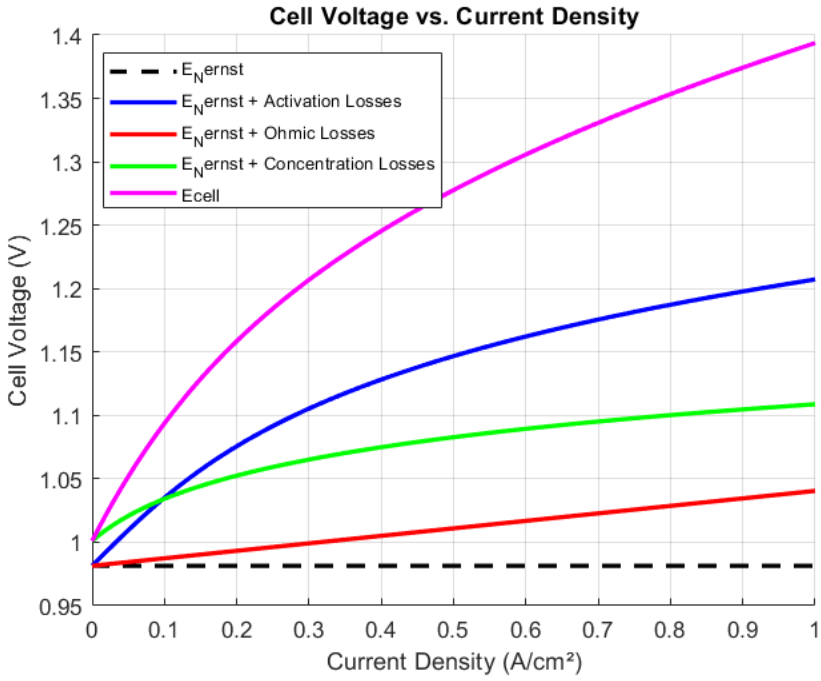

Figure 4.1: Cell potential and reversible losses as a function of current density.

Figure 4.1 illustrates the curves produced by the electrochemical model in Section 3.2 assuming a stream composition, both at the cathode and the anode, to be equal to those at the cell inlet. Therefore, it does not describe the entire SOEC model, but rather a predicament of the SOEC behaviour. It can be observed that the irreversible losses increase as

the current density also increases. This relationship satisfy the electrochemical kinetics of the electrolyser. Among these losses, only the ohmic loss exhibits a linear dependence on current density. During operation, activation losses are the most significant, followed by concentration losses, with ohmic losses being the smallest.

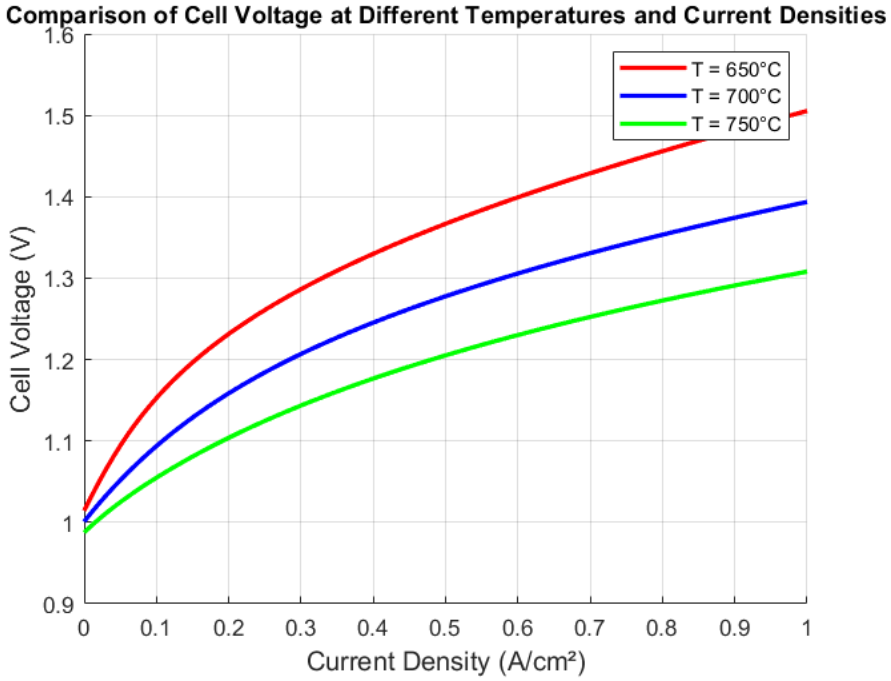

Figure 4.2: Cell voltage as a function of current density for different working temperatures

It is possible to analyse the impact of the current density on the cell voltage under different working temperatures. For a given current density, the cell voltage decreases as the temperature increases, due to enhanced electrochemical reaction kinetics and reduced overpotentials.

As mentioned in 3.2, if the cell voltage is equal to the thermoneutral voltage, there is no need to add nor extract heat from the stack, working solely on electrical energy. The figure below illustrates the influence of temperature on the cell voltage, with the current density chosen to correspond to the thermoneutral voltage condition for the operating conditions expressed in Table 3.2, predicted by the electrochemical model.

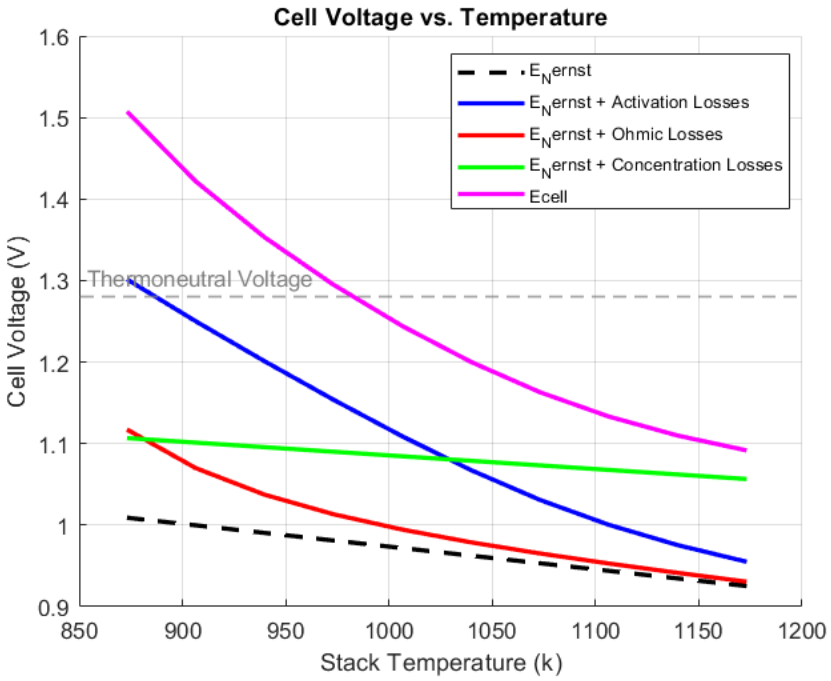

Figure 4.3: Cell potential and reversible losses as a function of temperature.

Figure 4.3 illustrates the impact of temperature on cell voltage and irreversible losses. It is evident that increasing temperature reduces the Nernst (reversible) potential while also decreasing irreversible losses due to improved reaction kinetics and thermodynamic efficiency. The activation losses are highly affected by the temperature since the H_2O electrolysis is an endothermic reaction. As the temperature rises, the activation energy required for the reaction decreases, leading to enhanced charge transfer kinetics. This results in lower activation losses, improving overall stack performance. However, while ohmic and concentration losses also decrease with temperature, their effect is less pronounced compared to activation losses.

As referred in Section 3.3, the cell is spatially discretized to analyse the evolution of temperature and molar fractions throughout its' length. The figures below help to visualize these changes in steady-state conditions, i.e., with constant current density.

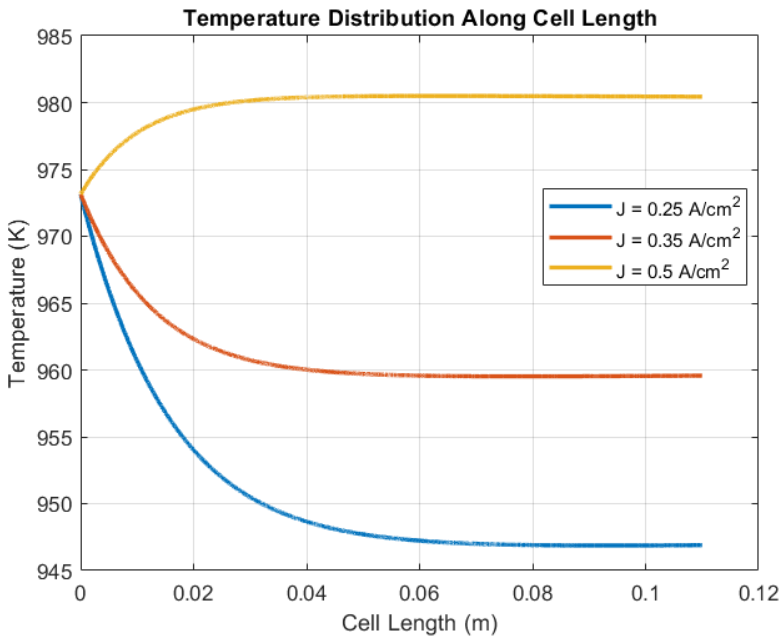

Figure 4.4: Temperature profile under different current densities.

The figure illustrates the temperature distribution along the SOEC stack for different current densities. It can be observed that an increase in the current density further increases the temperature along the cell, while a decrease in the current density results in a temperature drop. This behaviour arise from the energy balance in the cell: if the cell voltage does not reach the thermoneutral voltage, the electrolysis process is endothermic, thus, requiring heat input from the environment to maintain the working temperature.

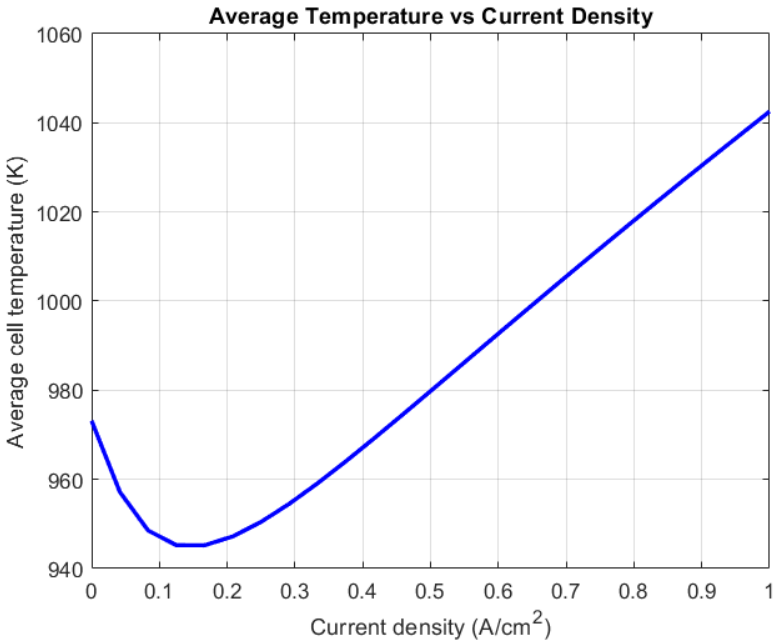

Figure 4.5: Average cell temperature as a function of current density.

The figure below illustrates the thermal energy required by the endothermic electrolysis process as a function of the current density, based on the operating conditions summarized in Table 3.2. From the analysis of Figure 4.5, it can be conclude that only at approximately 4500 A/m^2 do the irreversible losses generate sufficient heat to fully supply the thermal energy demanded by the electrolysis reaction, i.e., for the SOEC to work under thermoneutral conditions where the energy balance is zero. Beyond that threshold, the SOEC generates heat, leading to a temperature rise within the cell that must be managed through appropriate thermal control strategies to avoid material degradation and ensure stable operation.

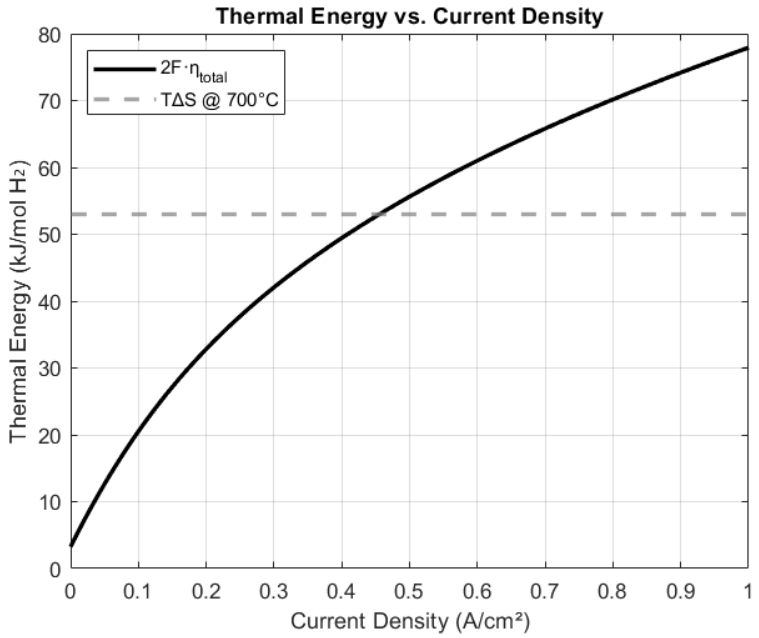

Figure 4.6: Thermal energy per mole of H2 consumed by the reaction and that produced by the irreversible losses, as a function of current density.

Analysing Figures 4.5 and 4.6, it can be observed that if temperature variations and their associated impact on cell voltage are not considered, the electrochemical model tends to overestimate the thermoneutral voltage. In both figures, the thermoneutral condition appears to occur at approximately 4500 A/m^2, whereas in Figure 4.1, this point is shifted closer to 6000 A/m^2.

Another parameter important to evaluate are the outlet stream compositions in terms of molar fractions, as these directly influence downstream processing and system integration. Figure 4.7 illustrates the molar fractions of the outlet species from the SOEC as a function of the applied current density. As expected, increasing the current density leads to higher molar fractions of the electrochemical products. This behaviour is in agreement with the trends predicted by Equations (3.20) and (3.21).

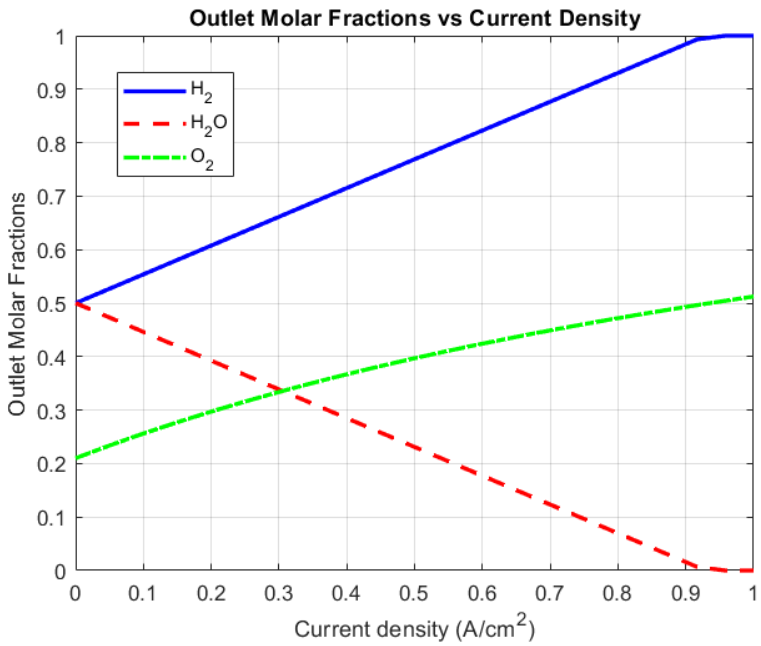

Figure 4.7: Species molar fractions at the outlet of the SOEC as a function of current density.

Another important parameter to consider when designing a SOEC is the *Steam Conversion* (SC), as discussed in Section 3.2. Figure 4.8 illustrates the SC as a function of current density, showing a behaviour consistent with Equation (3.22). As expected, SC increases proportionally with the input current, reflecting the direct relationship between electrochemical reaction rate and current density.

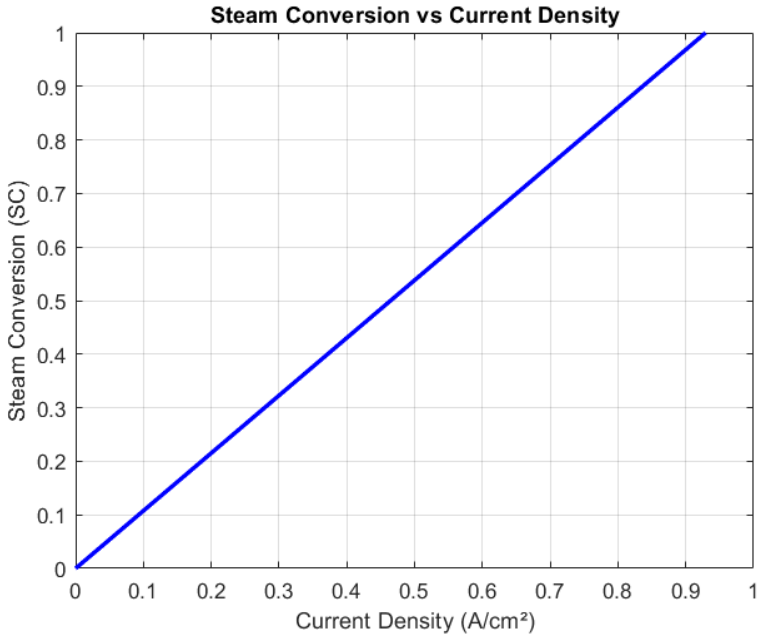

Figure 4.8: Steam conversion as a function of current density.

The efficiency of the SOEC, as depicted in the figures below, is determined using Equation (3.23). Since the H_2 produced through H_2O electrolysis does not have a predefined end use, the lower heating value (LHV) is considered instead of the higher heating value (HHV) [Smolinka and Garche, 2022].

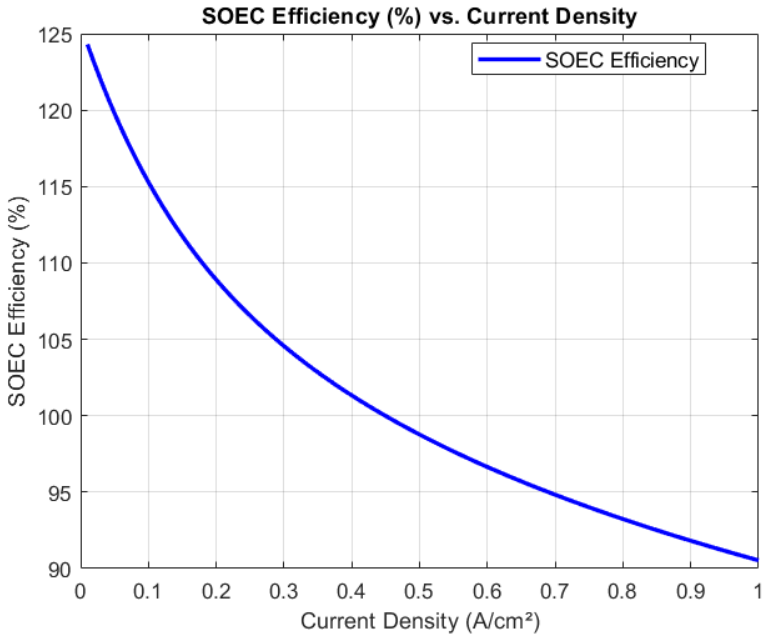

Figure 4.9: Stack efficiency as a function of current density.

The stack efficiency decreases as the current density increases. Since power input is directly proportional to the current, a rise in current leads to a corresponding increase in power consumption. This, in turn, results in a decline in stack efficiency. Moreover, the unusually high efficiency values exceeding 100 %, arise due to the definition of efficiency in Equation (3.23) . The calculation only accounts for the electrical power input, while part of the energy required for electrolysis is supplied by thermal energy. As such, the energy stored in the produced H_2 can exceed the electrical input alone, yielding efficiencies greater than 100 %.

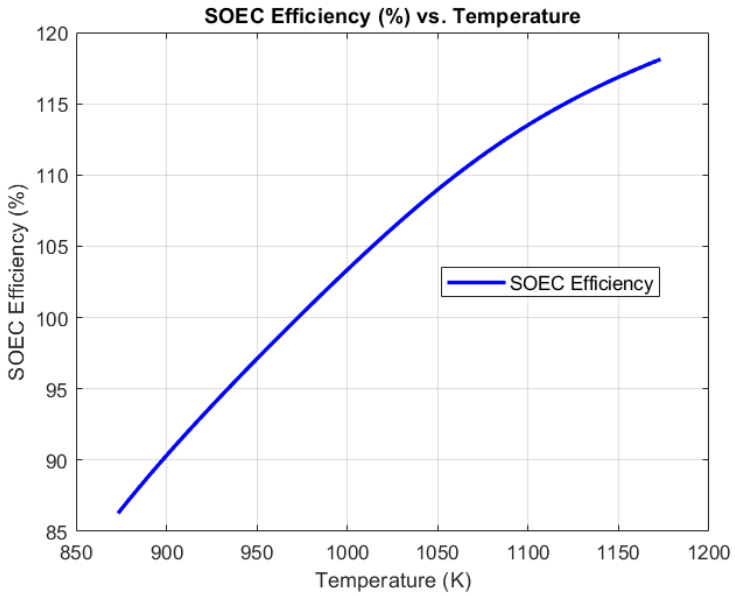

Figure 4.10: Stack efficiency as a function of temperature operating at the thermoneutral voltage.

It can be observed in Figure 4.10 that the stack efficiency increases with rising temperature. This phenomenon aligns with the principle previously illustrated in Figure 4.3 where the cell voltage decreases with increasing temperature. As mentioned earlier, higher temperatures reduce activation losses and improve electrochemical performance. Additionally, increased temperature enhances ionic conductivity within the electrolyte, leading to lower internal resistance and a lower cell voltage. This results in a higher efficiency as power input is directly proportional to the cell voltage.

4.1.1 Results Validation

To ensure the reliability and accuracy of the numerical model in the absence of experimental data, it is compared to values reported with literature under equivalent operating conditions and number of cells.

In order to accurately evaluate the system's behaviour under dynamic operation, characterized by load variations over time, a transient simulation replicating the conditions presented in the study [Wang et al., 2020] is performed, and its outputs are validated against the results of that study. To ensure a precise comparison, the literature data points are extracted to plot alongside the simulation results. This comparison is illustrated in Figures 4.11a and 4.11b, which show the evolution of total voltage and power over time, respectively. It is important to note that the current density is different for both models as the cell and stack configurations differ. However, the peak current reported in the study [Wang et al., 2020], is adopted in the present study to ensure a proper equivalency.

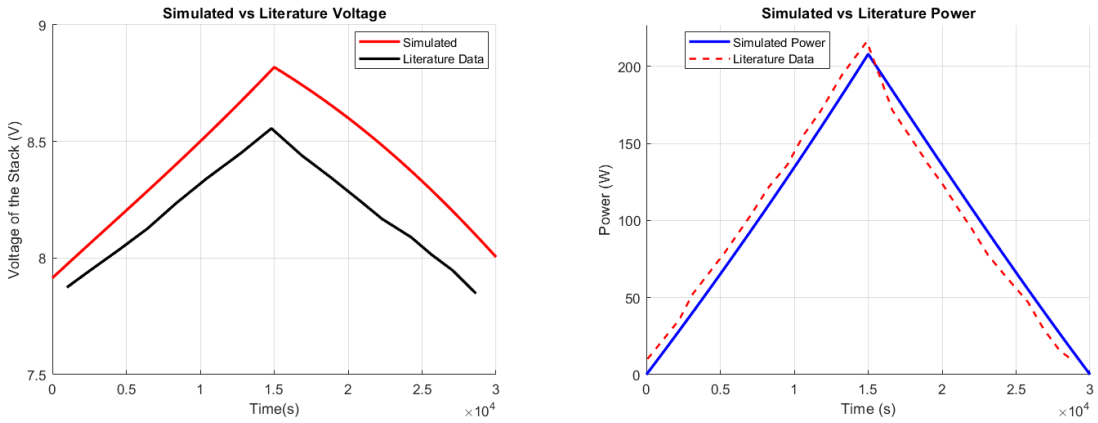

(a) Total voltage comparison over time.

(b) Power comparison over time.

Figure 4.11: Comparison between simulation and literature results under dynamic operation conditions.

The simulated voltage profile shows a good agreement with the literature, with a maximum error of 0.3416 V (or 4.14 %) occurring at $t = 20780.9$ s, where the simulated voltage was 8.5881 V and the reported literature value was 8.2465 V. Regarding the power profile, the maximum error reached 15.03 W (or 19.35 %) at $t = 23094.3$ s, corresponding to a simulated power of 92.74 W compared to 77.70 W from the literature. Although the power profile shows a higher relative error, the most critical parameter in evaluating the electrochemical performance is the total voltage, which demonstrates a reasonable and acceptable deviation.

From a steady state perspective point of view, multiple publications including those by [Ni et al., 2007], [Zhang et al., 2025], and [Hauck et al., 2017], report results that are consistent with those presented in Section 4.1. The trends observed in Figures 4.1 to 4.4, align closely with these studies, particularly regarding the influence of temperature and current density on the cell voltage. Naturally, minor discrepancies in the graphs arise due to differences in modelling approaches, operating conditions, and stack configurations.

The next section aims to provide results under dynamic conditions, evaluating the stack behaviour in response to step load changes are inserted. Additionally, the performance of HXs and electric heaters outputs is also evaluated.

4.2 Transient Performance

The performance of the stack under transient behaviour is highly dependent on its' design and operating parameters. In this study, several variables are analysed, including temperature and species concentration evolution, and the overall response of the stack to sudden load changes. To investigate these effects, a SIMULINK simulation with a total duration of 10 hours is performed, applying three different current density values throughout the simulation period. According to [Elcogen, 2025], the maximum nominal current for a single stack is 60.5 A, resulting in a total of 242 A for a series of four stacks.

The operating current densities applied in the simulation correspond to 75 %, 37.5 %, and 99.9 % of the maximum current. Although the choice of these values is arbitrary, it serves

the important purpose of evaluating the stack's behaviour under various load inputs and transition scenarios. The load changes are considered to be instantaneous, meaning they occur with no delay or ramping between steps.

Additionally, a supplementary study of the SOEC stack is performed under extreme conditions. The model outputs are expressed in Appendix A.

4.2.1 SOEC Dynamics

This subsection presents the dynamic behavior of the stack under the specified operating conditions. Several key parameters are analyzed and discussed, with corresponding plots provided to offer visual support and enhance the understanding of the phenomena occurring throughout the simulation.

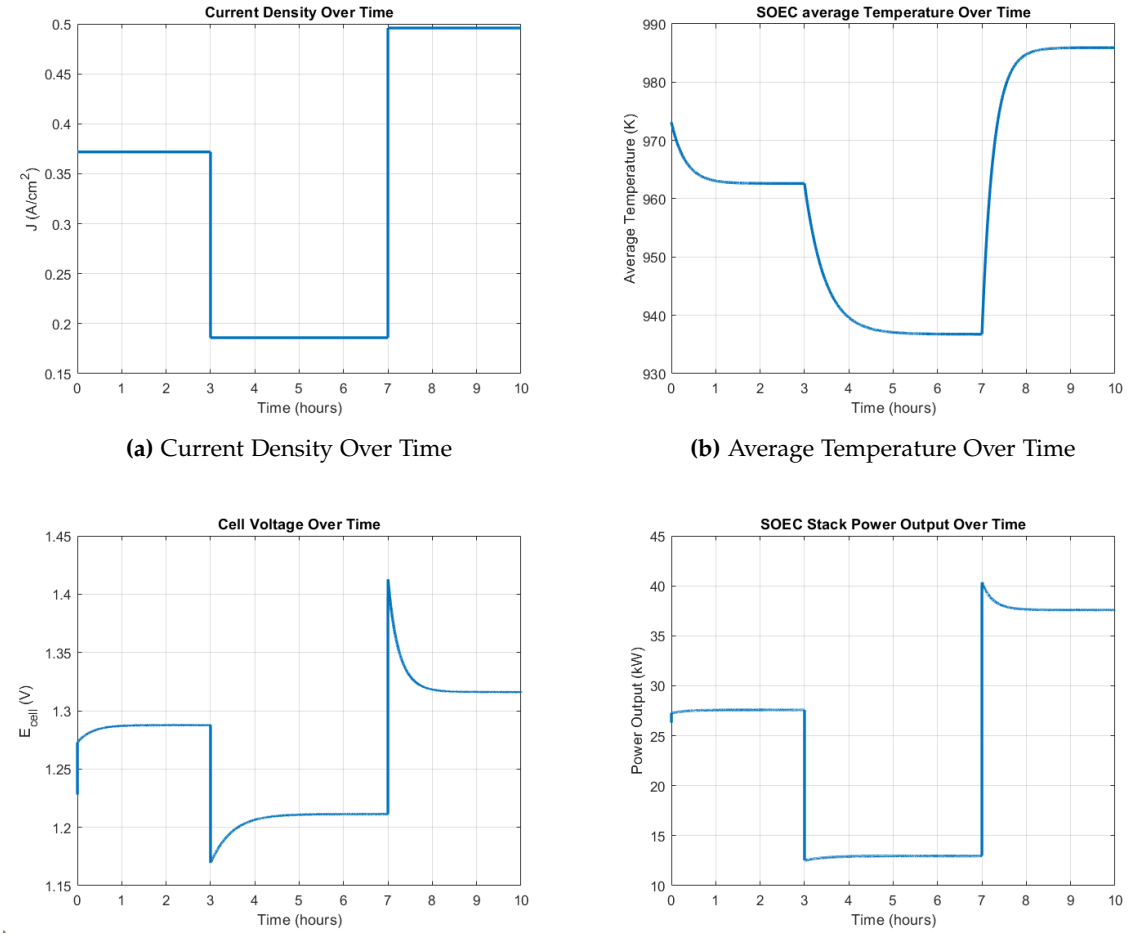

(a) Current Density Over Time

(b) Average Temperature Over Time

(c) Cell Voltage Over Time

(d) Power Output Over Time

Figure 4.12: Dynamic behaviour of the SOEC system under load changes.

The figures above illustrate the evolution of various stack parameters over time. Figure 4.12a shows the current density profile, highlighting the three load changes discussed earlier. As mentioned in Section 4.1, the stack reaches the thermoneutral voltage at approximately 0.45 A/cm^2, which explains the decrease in the stack's average temperature observed in Figure 4.12b. Only during the final load change does the temperature in-

crease, indicating net heat generation within the stack. The cell voltage profile spikes observed in Figure 4.12c are consistent with the electrochemical equations mentioned in Section 3.2. When the load suddenly increases, the overpotentials increase (as shown in Figure 4.1), while the temperature remains unchanged for a moment due to the thermal inertia. Hence, this mismatch leads to a temporary increased voltage. As the simulation progresses, the stack temperature gradually adjusts to the updated operating conditions, reducing the overpotentials (in agreement with the trends presented in Figure 4.3), and allowing the cell voltage to stabilize.

Another important parameter to analyze in a transient simulation is the composition of the exhaust gas from the SOEC. Additionally, SC is a key indicator, describing the fraction of H_2 vapour from the inlet mixture that is effectively converted into H_2. Figures 4.13a and 4.13b show exactly how these parameters evolve under step load changes.

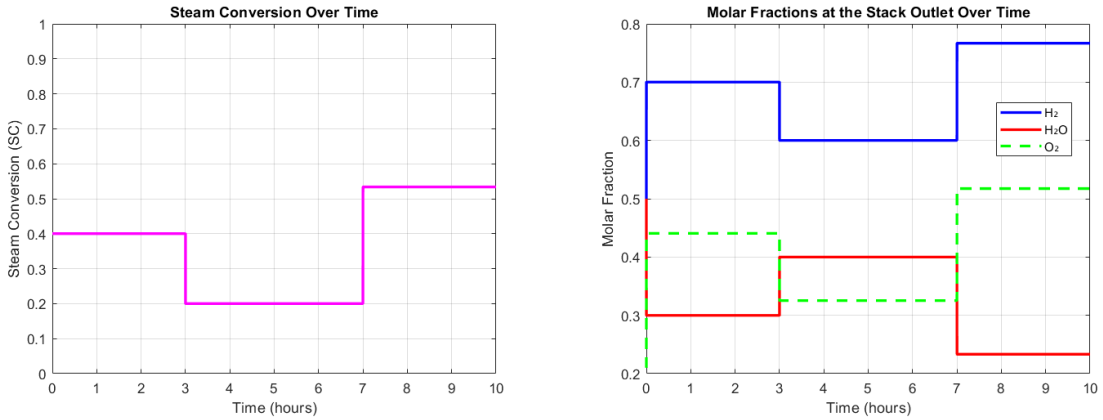

(a) Steam Conversion Over Time

(b) Molar Fractions Over Time

Figure 4.13: Species composition and SC under load changes.

It can be observed that both parameters respond instantaneously to the applied load changes. The trends shown in the figures are consistent with the behaviour predicted by Equations (3.22) and (3.24). An increase in current leads to a higher SC and a greater production of H_2, which in turn results in an increased H_2 molar fraction at the system outlet.

One of the main concerns with SOEC is the temperature gradients, which should ideally remain below 10 K/cm. High temperature gradients can lead to severe degradation mechanisms, including accelerated material ageing, thermal stress, cracking of the electrolyte and other system components, and eventual malfunction or failure of the cell.

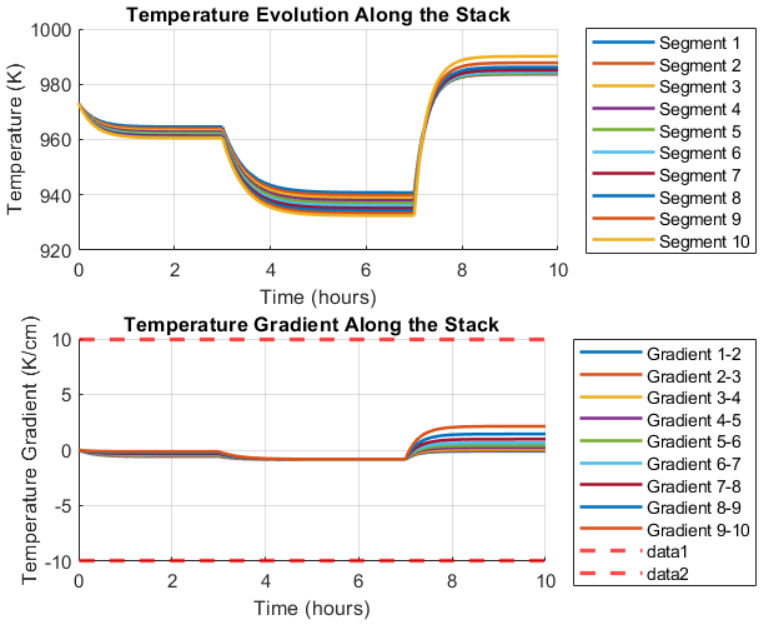

Figure 4.14: Temperature gradient across the cell over time

Figure 4.14 illustrates the temperature gradient during the entire simulation across the discretized cell, computed between each pair of adjacent segments. The discretization and temperature gradient calculation is performed using one segment and the one after. In the first load, the temperature gradient between nodes is low but its values vary differently. In contrast, during the second load, this temperature gradient is more uniform throughout the cell length leading to a more thin line as observed in the figure.

Figure 4.15 depicts a clearer temperature variation between segments over time. The temperature variation during the second load change is more uniform due to the lower current input, and therefore, a reduced electronic resistance. This results in a smoother temperature profile.

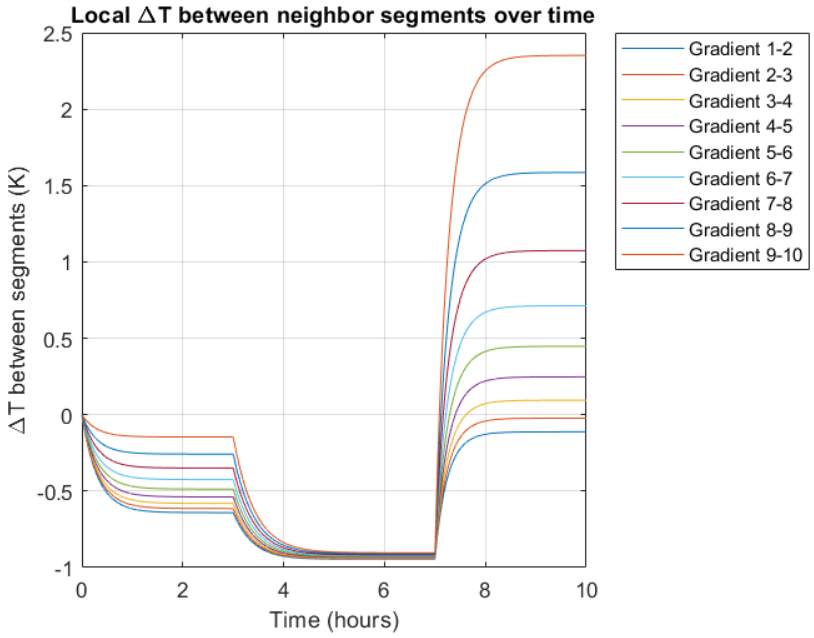

Figure 4.15: Local temperature variation between segments over time.

Figure 4.16 illustrates the temperature gradient between the inlet and the outlet of the cell, i.e., between the first and last segment. Despite the lower accuracy of the discretization compared to local segment-by-segment calculations, it provides a representative overview of the overall temperature gradient across the entire cell.

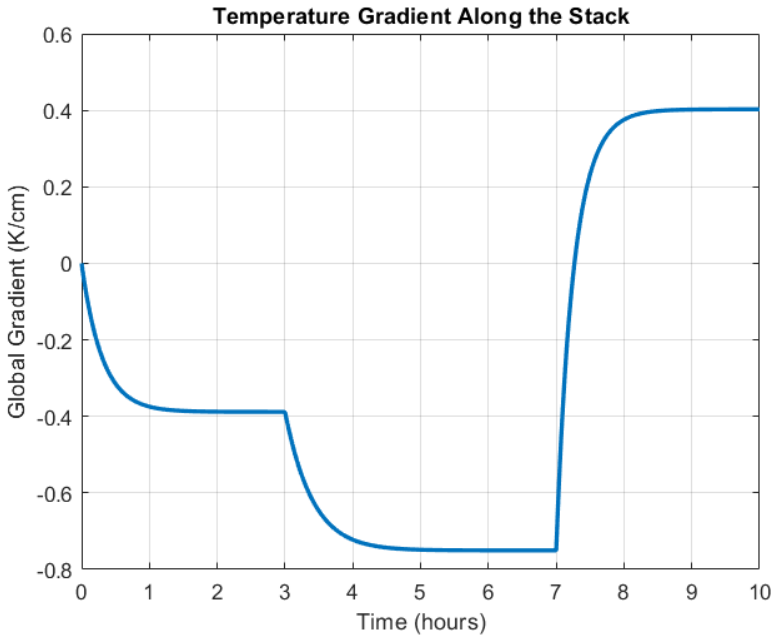

Figure 4.16: Overall temperature gradient between the inlet and outlet of the cell over time.

The figures above illustrate one of the main challenges when designing a SOEC system. Despite the presence of step load changes and the neglect of heat losses in the model, the results demonstrate that the temperature gradients remain within acceptable limits, thereby fulfilling this critical design constraint. Additionally, the model includes a temperature stabilization analysis after each load change. Specifically, it calculates the time required for the temperature variation across any segment of the cell to remain within 1 K over a 10 minute window. Following the first load change, the stack stabilized after approximately 35 minutes; after the second load change, stabilization occurred after 1 hour; and following the final load change, stabilization was achieved after 57 minutes.
This analysis is beneficial for effectively assessing and understanding the time required for the SOEC to reach thermal steady-state following operational changes.

Another key performance indicator to assess in a transient SOEC simulation is the *Specific Energy Consumption* (SEC), which measures the energy required to produce a unit mass of H_2. Figure 4.17 presents the time evolution of the SEC in response to the stepwise load changes applied on the system. This parameter provides direct insight into the energy efficiency of the electrolyser under dynamic operating conditions, making it crucial for evaluating overall system performance.

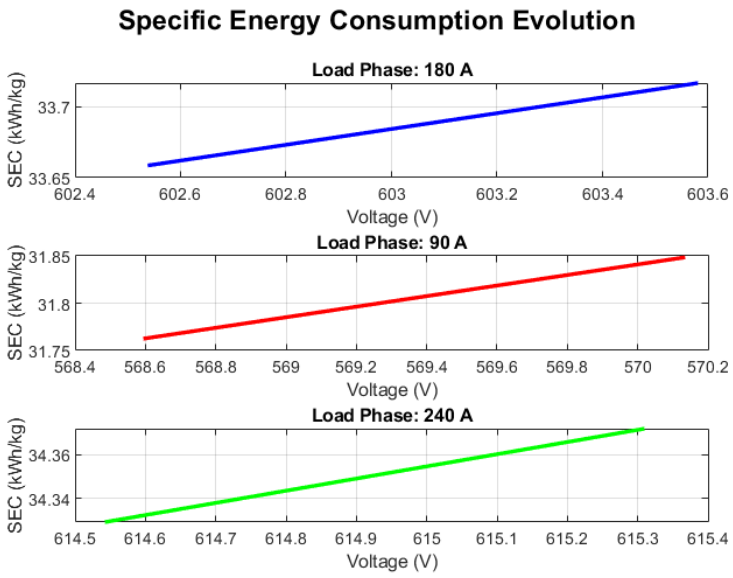

Figure 4.17: Specific Energy Consumption evolution under load changes.

The figure above illustrates the SEC evolution under different load changes after stabilization. As previously discussed and shown in Figure 4.12c, the voltage spikes observed during load transitions directly affect the SEC values. For this reason, the SEC is calculated only after the stack voltage stabilizes at each new load condition.

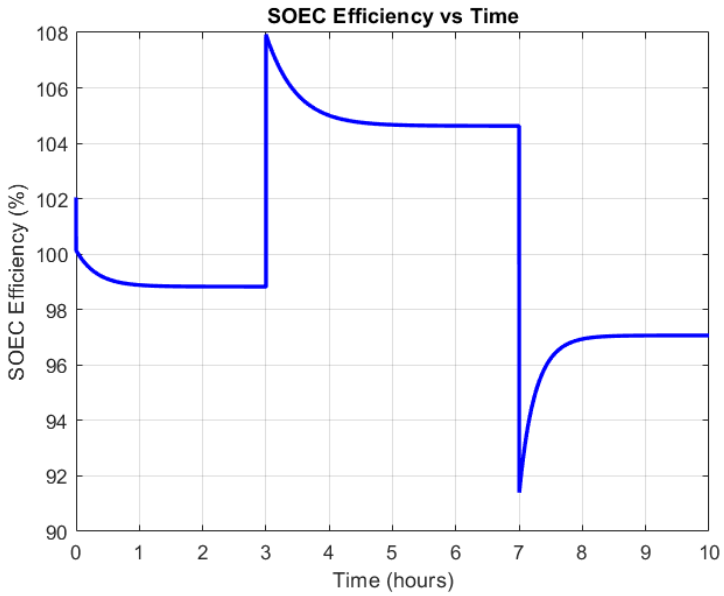

Figure 4.18: SOEC efficiency over time.

Figure 4.18 illustrates the SOEC efficiency over time. The high efficiency values, as previously discussed in Section 4.1, result from considering only the electrical power input, as in Equation (3.23), while neglecting the thermal energy contribution that also takes part on the electrolysis reaction.

4.2.2 Heat Exchangers

As explained in Section 3.5, both the HXs of the present model are designed using the LMTD method. The figures below illustrate the required power consumption to properly exchange the heat transfer between fluids.

Fuel HX

The fuel side HX is responsible for increasing the inlet stream temperature close to the working temperature of the SOEC. The cold stream is the steam mixture and the hot stream is the exhaust gas from the SOEC. The hot stream temperature profile is shown in Figure 4.16.

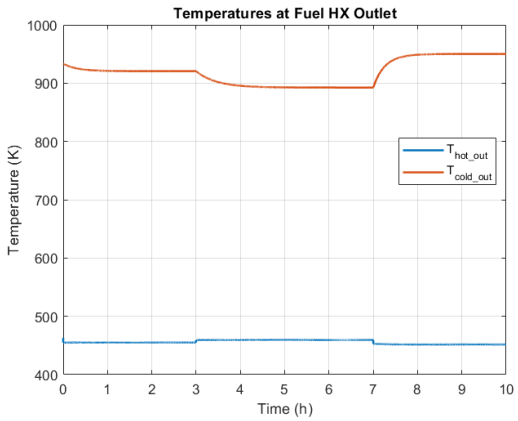

(a) Hot and cold streams outlet temperature over time

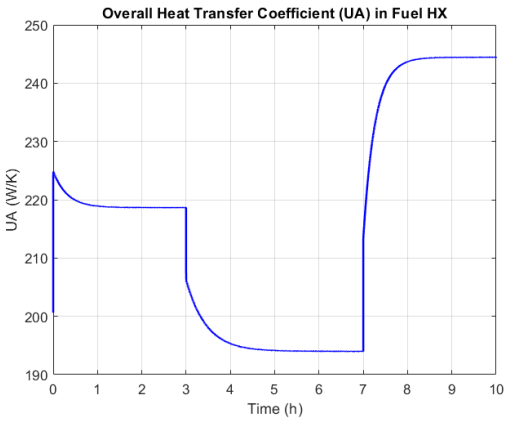

(b) Overall Heat Transfer Coefficient over time

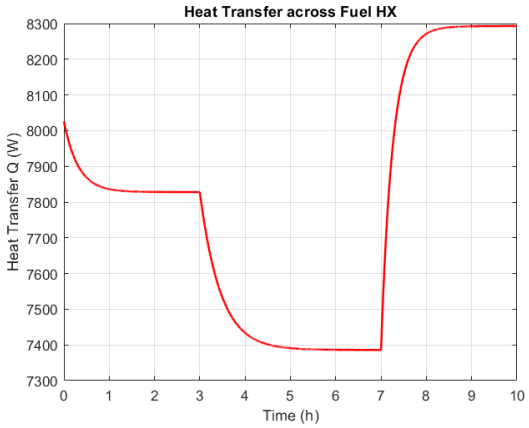

(c) Heat transfer rate over time

Figure 4.19: Dynamic behaviour of the fuel HX unit during operation.

Figure 4.19 illustrates the behaviour of the fuel side HX over the simulation period. As expected, the cold stream outlet temperature exhibits a 40 K difference compared to the SOEC exhaust, as explained in Section 3.5. The hot stream outlet temperature reaches a maximum temperature of 460 K which must be later processed to condense the H_2O present in the gas stream and extract the H_2. The UA value reaches its peak value under the highest operating conditions, with an approximate value of 245 W/K. Additionally, the heat transfer rate achieves values as high as 8300 W, which is consistent with the significant thermal energy exchange occurring between the cold and hot streams.

Air HX

The air side HX is responsible for heating the anode inlet gas to match the operating temperature of the SOEC. This process helps to minimize temperature gradients across the cell, thereby ensuring safe operation and extending the system's lifetime.

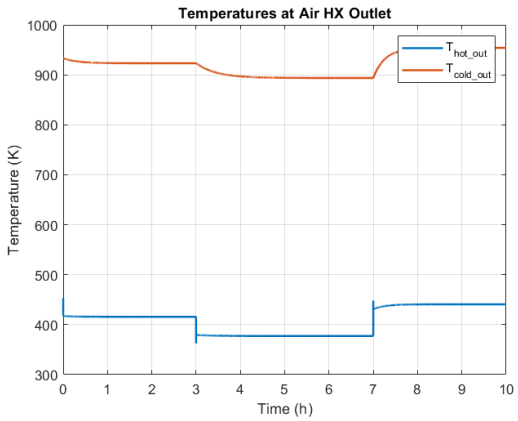

(a) Hot and cold streams outlet temperature over time

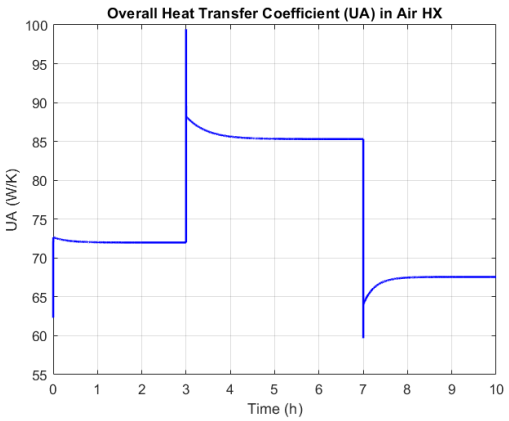

(b) Overall Heat Transfer Coefficient over time

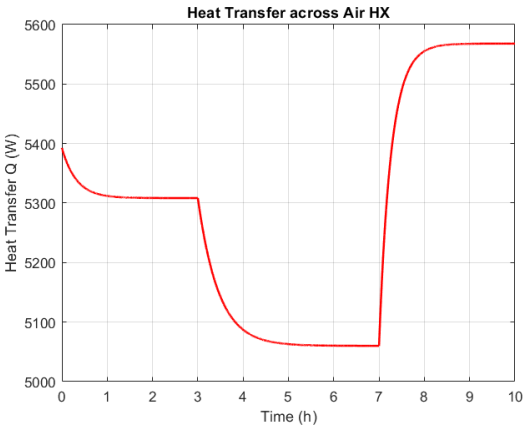

(c) Heat transfer rate over time

Figure 4.20: Dynamic behaviour of the air HX unit during operation.

Figure 4.20 shows the dynamic behaviour of the air HX under different load changes. Similar to the fuel side HX, the pinch point is maintained constant, and the cathode exhaust gas temperature is assumed to match that of the anode, resulting in a temperature profile identical to the one in Figure 4.19a. Regarding the UA value, the spikes in the plot appear to have the same behaviour as the cell voltage's, discussed in Section 4.2.1. Consequently, the proper maximum value is approximately 90 W/K. Finally, the heat transfer rate reaches its peak during the final load change, as observed for the fuel side HX, with an approximate value of 5600 W.

4.2.3 Electric Heaters

The use of electric heaters it to match the cold stream outlet temperature of both HXs to the working temperature of the SOEC. Since the difference between these two temperatures is low (pinch point), the electric heater power is relatively small in comparison to the rest of the system.

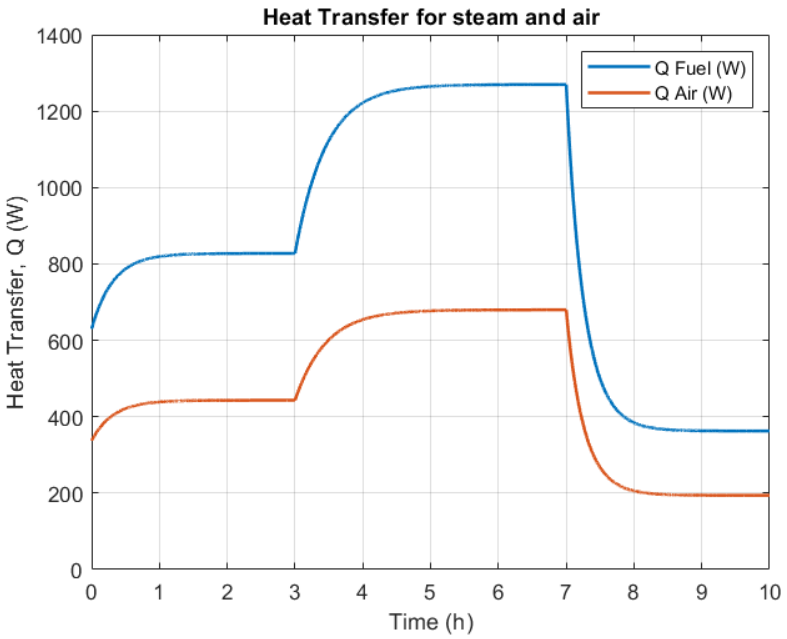

Figure 4.21: Heat transfer for both fluids to match the SOEC working temperature.

Figure 4.21 illustrates the required electrical energy to increase the steam and air temperatures, after the HX units, to the SOEC operating temperature. As discussed previously, the cathode stream requires more energy due to its higher molar flow rate. The highest heating demand occurs during the second load step, where the lower current results in reduced internal heat generation, thereby increasing the reliance on external heating to reach the desired temperature.

4.2.4 System Efficiency

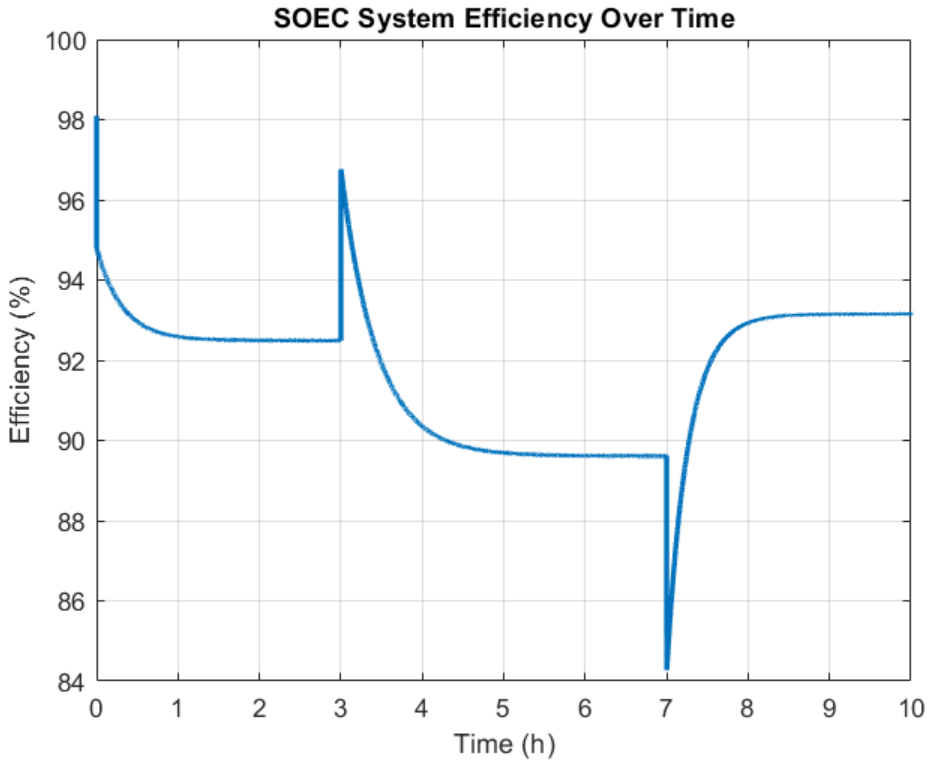

Figure 4.22: System Efficiency over time

Now, with the outputs of each component available, it becomes possible to evaluate the overall system efficiency under transient operating conditions. The system efficiency is continuously calculated throughout the simulation using Equation (3.36), which accounts for the dynamic evolution of the process variables over time. The spikes observed in the figure are a reflection of the cell behaviour in Figure 4.12c. Since the efficiency is inversely proportional to the power input, the behaviour is similar. The maximum system efficiency is achieved during the final load change, attaining approximately 93 %.

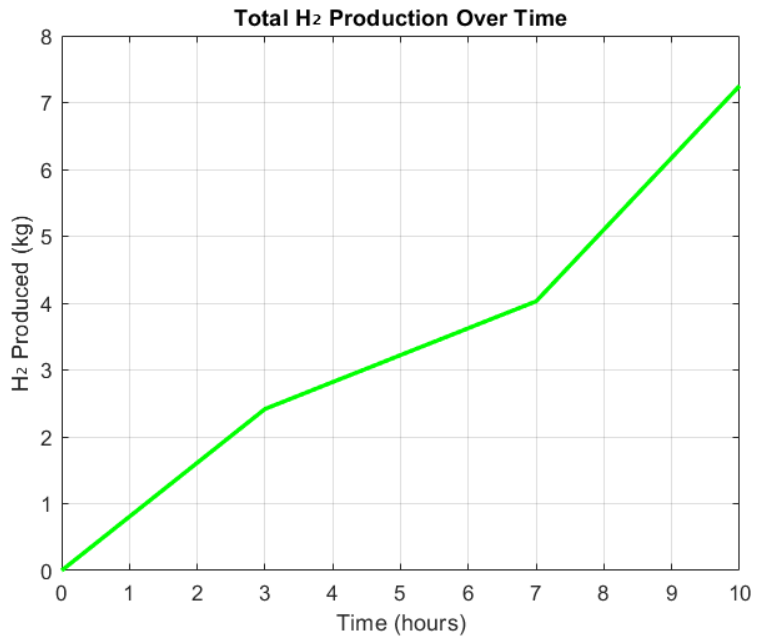

Figure 4.23: H_2 production over time

The present study consists of a 10 hour electrolysis process following different load changes. Figure 4.23 illustrates the cumulative production of H_2 during this period reaching a total weight of 7.25 kg in the end of the simulation. This amount is calculated following Equation (3.20).

4.3 Sensitive Analysis

Operating Pressure

Pressure is a key operating parameter in SOECs, as increasing it enhances the molar diffusion rate and reduces concentration losses, thereby lowering the cell voltage. However, increasing pressure leads to a rise in the non-standard conditions cell voltage as a result of the Nernst Equation (3.7). Figure 4.24 illustrates the pressure impact under different increasing values.

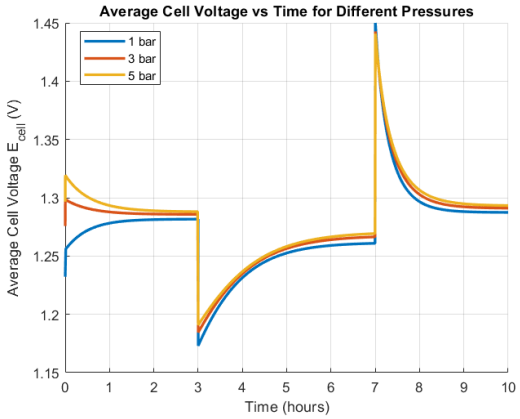

(a) Cell Voltage over time under different operating pressures.

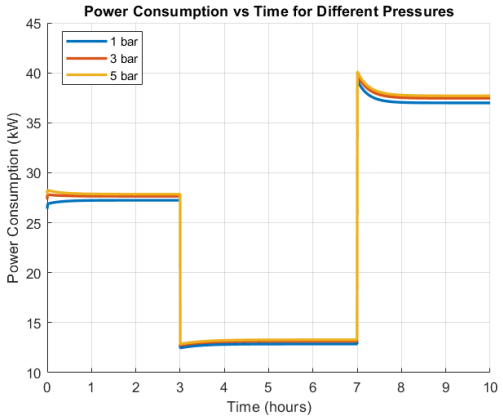

(b) Power Consumption over time under different operating pressures.

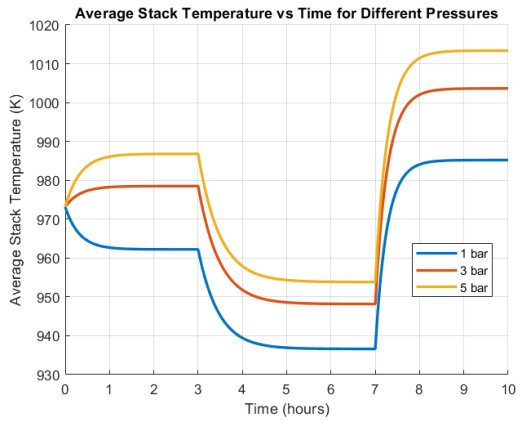

(c) Average Stack Temperature over time under different operating pressures.

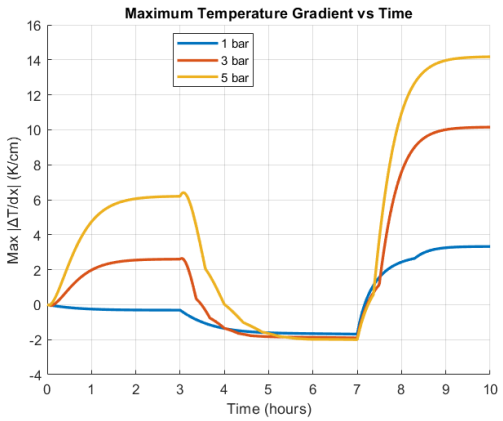

(d) Temperature Gradient over time under different operating pressures.

Figure 4.24: Dynamic behaviour of the SOEC system under different operating pressures.

The figure above illustrates the pressure impact on the SOEC operation. Under the specified conditions, increasing pressure leads to a worse system performance, as evidenced by higher cell voltages, elevated temperatures, and a maximum temperature gradient that exceeds the 10 K/cm constraint. This indicates that the increase in pressure is not sufficient to enhance the diffusion rates, and therefore decrease the concentration overpotentials. According to [Ni et al., 2007], the benefits of operating at higher pressures become significant only above current densities of 0.5 A/cm^2 with cathode-supported SOECs. Below this threshold, a working pressure of 1 bar is recommended. Since the SOEC stack in the present model does not surpass that current density threshold, the advantages are negligible. Moreover, higher operating pressures require additional electrical energy, which can ultimately reduce the overall system efficiency.

Effect of Inlet Gas Composition

Sections 4.1 and 4.2 illustrate the results under constant inlet gas composition. However, variations in the H_2O/H_2 ratio at the inlet can significantly affect the stack's thermal and electrochemical behaviour. The following figures show the system's response to the same step load changes as in the previous sections, but for different inlet gas compositions.

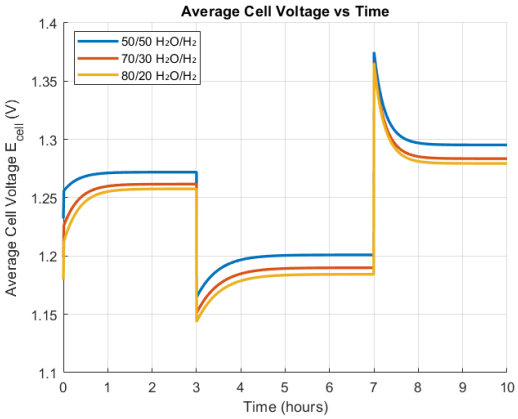

(a) Average Cell Voltage Over Time

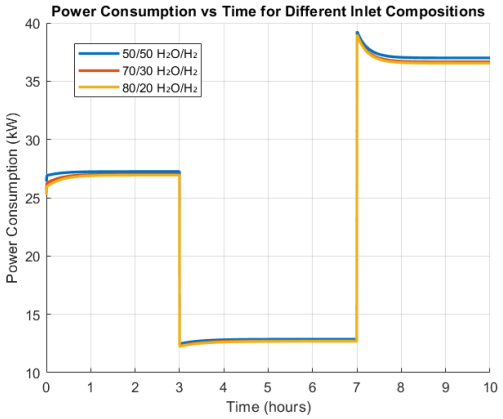

(b) Stack Power Over Time

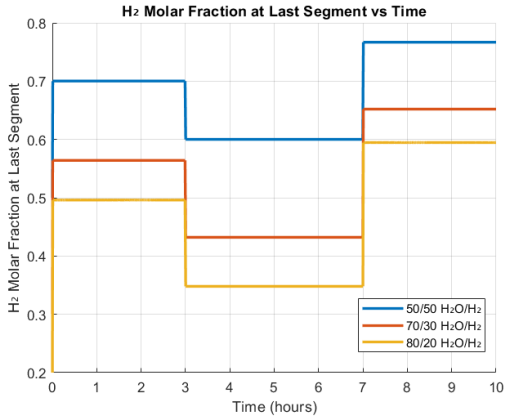

(c) Outlet Molar Fractions Over Time

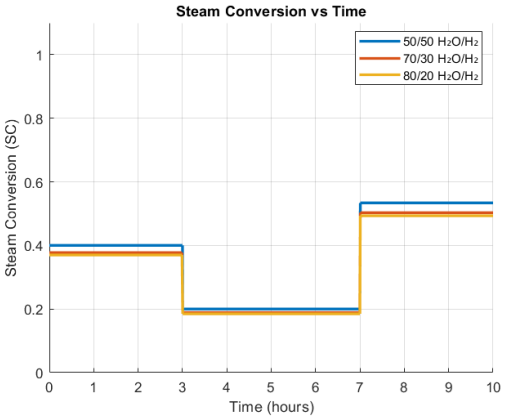

(d) Steam Conversion Over Time

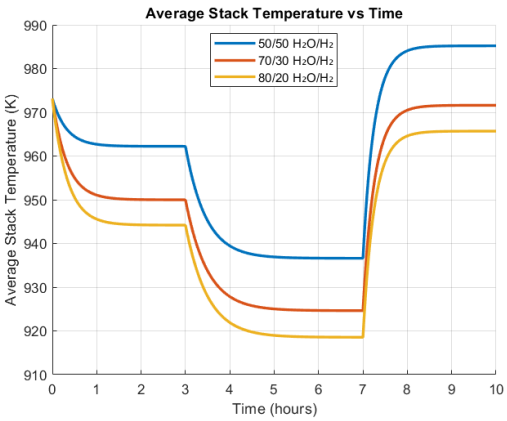

(e) Average Stack Temperature Over Time

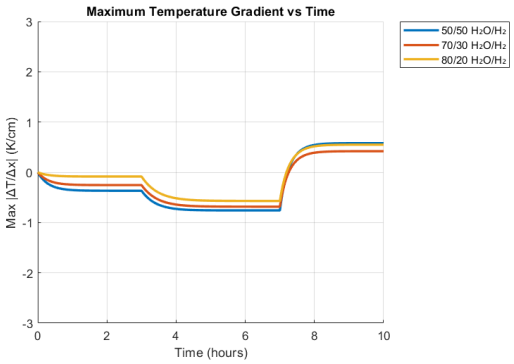

(f) Maximum Temperature gradient over Time

Figure 4.25: Dynamic behaviour of the SOEC system under different inlet gas compositions.

Figure 4.25 illustrates the impact of varying inlet gas compositions on the main dynamic performance indicators of the SOEC system. It can be observed that a lower H_2 content in the inlet mixture results in a reduced cell voltage, leading to lower power consumption and a decrease in the average stack temperature. This temperature reduction is primarily attributed to the higher H_2O fraction in the feed, which increases the thermal mass and

lowers the outlet gas temperature due to its higher specific heat capacity. Although the difference between the outlet and inlet H_2 fractions is more pronounced for the 80/20 ratio, the resulting SC is lower, as shown in Figure 4.25d. This behaviour aligns with Equation (3.22), where a higher H_2O fraction in the feed increases the denominator, thereby lowering the SC value even if the absolute H_2 production remains high.

For the temperature gradient, although the overall temperature drop is more pronounced with increasing H_2O content, the resulting gradient is smaller. This occurs because the temperature decrease is more uniformly distributed along the cell, leading to a smoother thermal profile compared to the scenario discussed in Section 4.2.

Chapter 5

Discussion

In this section, various aspects of the SOEC system are discussed including sustainability, operational limits, dynamic behaviour, components sizing, economic impact, assumptions in the model, and system efficiency. The analysis of these aspects aims to assess whether such a system is viable and effective in real life applications.

Sustainability

Section 1 highlights the urge to reduce the GHG emissions in response to the global warming and its associated consequences. One of the many benefits of SOECs, contributing to this goal, is the nature of its byproducts, namely hydrogen and oxygen. These two substances, while abundantly available in nature, are also extremely valuable for various industrial and energy applications. Furthermore, SOECs demonstrate remarkable fuel flexibility, being capable of utilizing a wide range of feedstocks, including toxic or low-quality gases such as carbon monoxide. Their inherent reversibility allows them to function either as electrolysis cells or as fuel cells, depending on the system requirements. The material composition of SOECs typically relies on abundant and inexpensive elements contributing to their economic viability. These characteristics make SOECs highly versatile, not only for hydrogen production but also for syngas generation, carbon dioxide reduction processes, and integration into renewable energy storage and power-to-gas systems. As a result, SOEC technology presents a promising path for the development of a sustainable, low-carbon energy economy.
However, SOECs are still considered an expensive system, largely due to the significant thermal energy demand. If they're not connected to a heat source, such as industrial waste heat or a concentrated solar power plant, for example, their overall efficiency and economic viability is significantly reduced. Hence, the integration of SOECs with external heat recovery systems becomes critical for maximizing their potential benefits. By combining external heat recovery with renewable electricity sources such as wind energy, SOEC systems can achieve outstanding levels of efficiency, sustainability, and economic feasibility.

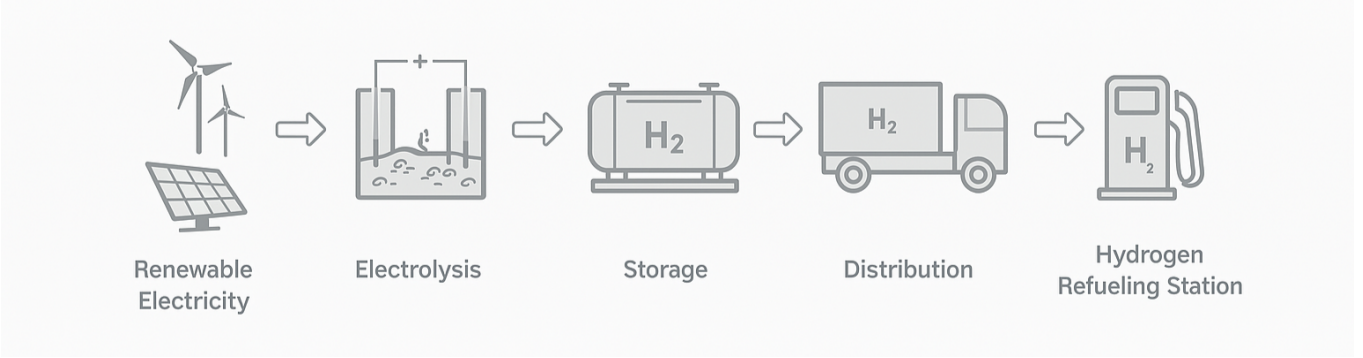

Figure 5.1: Renewable energy transformation pathway for hydrogen. Inspired by [Araya et al., 2020].

Operational Limits

The SOEC system operating conditions are highly limited by the maximum nominal current input. As referred in Section 4.2, the manufacturer indicates that the maximum current input per stack is 60.5 A. This is equivalent to a maximum current density of 0.5 A/cm^2 as the active cell area is 121 cm^2. The choice of the operating conditions depends on multiple parameters such as electric energy input, specific amount of produced hydrogen, incorporation of external heat source, etc.
Usually, SOEC stacks are preferred to work below thermoneutral conditions, in terms of operational cost and efficiency, resulting in an endothermic operation, which is often supported by heat integration [Udagawa et al., 2007]. The choice of operating conditions is a trade-off between energy efficiency, hydrogen production rate, and thermal management requirements. Working with low current densities typically leads to higher energy efficiency and reduced degradation rates, as the stack operates closer to the reversible voltage with lower overpotentials and thermal stresses. However, it results in lower hydrogen production rates and may increase the specific cost of the produced hydrogen due to the larger required stack size and longer operating times. In contrast, operating at high current densities allows for higher hydrogen production rates and more compact system designs, but it comes at the expense of increased overpotentials, reduced energy efficiency, and potentially accelerated material degradation due to higher thermal gradients and operating stresses.

In the present model, the system achieved the highest efficiency at the maximum current density permitted. However, simplifying assumptions such as adiabatic conditions, zero-dimensional representations of the HXs, and the absence of experimental validation may lead to an overestimation of the system's performance.

Dynamic Behaviour

The transient behaviour of the SOEC system was analysed under varying current densities, simulating operational changes over time. Changes in current led to variations in temperature, efficiency, and hydrogen production across the stack. Temperature stabilization after load changes was evaluated based on the gradient at the last segment, with stabilization defined as temperature variations below 1 K over a 10-minute period. After each load change, the system required between 30 and 60 minutes to reach thermal equilibrium, which is critical for control strategies and for integrating SOECs with intermittent renewable energy sources. It is important to highlight that the system's transient behaviour could differ if internal heat transfer mechanisms, such as conduction and radiation within the stack, and non-adiabatic conditions were included in the energy balance. Throughout transient operation, temperature gradients remained within safe limits (below 10 K/cm), minimizing the risk of thermal stresses and mechanical degradation. However, it should be noted that the step load changes applied in the model are idealized and do not fully represent real-life applications, where load variations are typically more gradual, and subject to noise and system inertia.

Additionally, the present study does not consider start-up or shutdown phases of the SOEC, which are also critical operating conditions. These phases significantly influence degradation rates and system lifetime, and should be included in future work to provide a more comprehensive understanding of long-term system performance.

The sensitive analysis performed with varying inlet gas compositions showed the inherent stack's change of behaviour. The most affected parameter was the average stack temperature, which, despite the variations, remained within the 10 K/cm thermal gradient constraint, an essential requirement in SOEC system design. From an economic perspective, the 80/20 H_2/H_2O ratio appears to be the most favourable inlet gas composition, offering a balance between system performance and hydrogen production efficiency. However, it is important to note that the model was developed based on a series of simplifying assumptions, such as ideal gas behavior, isobaric and adiabatic conditions, and neglect of pressure drops and heat losses. These assumptions, while useful for simulation purposes, may lead to deviations when compared to real-world system performance.

Adiabatic and Isobaric Conditions

The assumption of adiabatic and isobaric conditions, that the system does not exchange heat with its surroundings and operates at constant pressure, respectively, can significantly overestimate the efficiency and performance of SOECs. While these simplifications are useful for initial modelling, they do not fully represent real-world applications, where heat losses and pressure variations are inevitable, and must be accounted for during system design. The addition of conduction and radiation heat transfer within the SOEC stack requires detailed knowledge of the thermal properties of the materials involved, which are not available in this study due to confidentiality constraints. Furthermore, under the operating conditions considered in this project, pressure drops across the flow channels are typically small and can be neglected, as supported by [Udagawa et al., 2007].

Component sizing and Economic Impact

The main focus of this project was to investigate the dynamic behaviour of the SOEC under transient conditions, particularly in response to step load changes. As such, detailed component sizing and the associated economic implications were not within the scope of this work. However, some relevant design considerations emerged. For instance, the imposed pinch point temperature difference of 40 K between the heat exchangers (HXs) and the SOEC exhaust necessitated large overall heat transfer coefficients (UA values) for the HXs. However, this constraint could be relaxed by integrating an external thermal energy source, such as waste heat or a dedicated burner, to preheat the feed streams. The addition of external heat would reduce the required heat duty on the HXs, enabling more practical sizing and improving the system's economic viability. Although economic analysis was beyond the scope of this project, it is clear that thermal integration strategies play a key role in bridging the gap between theoretical performance and real-world feasibility.

Efficiency

Although this is a simplified model compared to real-world SOEC systems, which include auxiliary components such as pumps, compressors, condensers, and steam generators, the overall system electrical efficiency obtained is consistent with results from similar projects, such as the work by [Petipas et al., 2013]. However, the omission of thermal losses, assumptions made in the model, and stack degradation effects means that the simulated efficiency values should be interpreted as upper bounds. In practice, these factors reduce the net system efficiency and must be accounted for in a full techno-economic analysis. Furthermore, the use of an isobaric and adiabatic model can overestimate performance by neglecting the energy required for heating, pressurization, or system startup. Nevertheless, the results demonstrate that under ideal conditions, the system can achieve high efficiency across a range of operating currents. This confirms the potential of SOECs for integration into future power-to-gas or renewable hydrogen systems, provided that proper thermal management and component-level optimization are implemented

Chapter 6

Conclusion

This thesis presents the design and dynamic modelling of a 40 kW Solid Oxide Electrolysis Cell (SOEC) system, aimed at evaluating its performance under both steady-state and transient operating conditions. The developed model, implemented in MATLAB and Simulink, includes detailed electrochemical, thermal, and mass transport dynamics, along with auxiliary components such as heat exchangers and electric heaters.
The simulation results indicate that the SOEC system can achieve high efficiencies under idealized conditions, particularly when operating close to thermoneutral voltage. The temperature gradient along the cell remained within the critical 10 K/cm threshold throughout all load changes, satisfying key design requirements for system stability and longevity. The model also demonstrated a strong correlation with available literature, validating its reliability despite the absence of experimental data.

Under transient conditions, the system responded predictably to stepwise variations in current density. Temperature stabilization times varied between 30 to 60 minutes depending on the load, and hydrogen production increased proportionally with current input. The efficiency, species evolution, and energy consumption metrics followed expected trends, reinforcing the model's consistency.
A sensitivity analysis on inlet gas composition revealed that the thermal and electrochemical performance of the stack is highly influenced by the H_2/H_2O ratio. The 80/20 mixture led to a substantiable reduction in average stack temperature due to the higher thermal mass of water in the feed. Despite this, it showed improved voltage behaviour and reduced power consumption. These findings suggest that selecting an appropriate inlet gas composition is essential to optimize the trade-offs between thermal management, hydrogen yield, and system efficiency.
Furthermore, a sensitivity analysis on the operating pressure indicated that, under the specified conditions, increasing the pressure led to a decrease in SOEC system performance. However, systems operating under higher working conditions, i.e., under high current densities, could potentially benefit from pressurized operation.

The system electrical efficiency reached a peak of approximately 93 % during transient operation and remained above 80 % throughout most scenarios. The stack efficiency, as defined based solely on electrical input, exceeded 100 %. However, such values should be interpreted with caution, as they result from idealized model assumptions and do not account for real-world losses or auxiliary power consumption.

The most influential parameters were current density, inlet gas composition, and stack temperature. Higher current densities increased hydrogen output but reduced efficiency due to increased overpotentials.

During load transitions, the stack temperature, cell voltage, and specific energy consumption (SEC) were most impacted. Voltage spikes and heat imbalance affected performance temporarily until thermal equilibrium was restored.
Nonetheless, the model is based on key simplifying assumptions, such as adiabatic and isobaric conditions, ideal gas behaviour, and negligible heat losses. While useful for understanding fundamental dynamics, these assumptions may lead to overestimated performance. Future models should integrate more realistic boundary conditions, degradation mechanisms, and component-level heat transfer dynamics to approach real-world accuracy.

In summary, this study confirms the potential of SOEC technology as a high-efficiency hydrogen production pathway when supported by proper thermal management and operating strategies. The presented model serves as a valuable tool for further optimization and integration studies in renewable energy systems.

Chapter 7

Future Work

After reviewing the present project, there are several opportunities to further improve it in terms of accuracy, reliability and comprehensiveness. The following aspects could be addressed in future work to strengthen the model's realism and expand its technical scope.

Experimental Validation

The current model was validated against existing literature data. However, validation against experimental results from a physical SOEC setup would represent a major step forward. Such validation would allow for the calibration of model parameters using realistic data and reveal discrepancies that may not be captured through simulation alone. This would improve the model's predictive accuracy and ensure that the dynamic behaviour, particularly under transient conditions, aligns with actual system responses.

Start-up and Shutdown Phases

The present model only considered dynamic conditions involving load variations over time, without accounting for start-up or shutdown phases. Including these phases would significantly enhance the depth of the analysis, as SOECs are highly sensitive to thermal stresses caused by rapid temperature changes. To ensure long-term durability and avoid degradation, both start-up and shutdown must be carried out gradually, with controlled heating and cooling rates. These operational phases have a considerable impact on the overall efficiency and lifespan of the system. Incorporating them into the model would expand its scope and improve the level of detail, making it more representative of real-world operation and more suitable for practical implementation strategies.

Increased accuracy of the model

In engineering practice, the use of assumptions is common and often necessary to simplify complex systems into computationally manageable models. However, it is essential that these assumptions remain reasonable and do not significantly affect the core physical behaviour of the system. As discussed in Section 3, the present model incorporates several assumptions which likely contribute to an overestimation of performance when compared to real world operation. Despite this, such assumptions are valuable for gaining fundamental insight into the system's behaviour and for enabling preliminary analysis.
A model without these simplifications would demand significantly more computational time and require highly detailed information about each system component, which is often unavailable during early-stage development. Nevertheless, for the model to be implemented in a real-world application, the number and extent of assumptions must be minimized. Only through a more detailed and assumption-free representation can the model achieve the level of accuracy and reliability necessary for practical deployment.

System Reliability

Numerous studies focus on, or incorporate, the degradation rate of SOEC stacks. Including this aspect in the present model would significantly improve the depth of analysis by providing insight into the operating conditions that accelerate degradation. Such an extension would enable the evaluation of strategies to prolong the lifespan of the system and identify optimal conditions that minimize performance loss over time. Understanding degradation dynamics is essential for assessing long-term reliability and planning maintenance or replacement intervals in real-world applications. However, conducting such a study would require access to a physical SOEC setup in order to extract the necessary degradation data and validate the model accordingly.

Bibliography

[Alsagr et al., 2024] Alsagr, N., Ozturk, I., and Usman, A. (2024). Digital government, political stability, and nuclear energy investment: The role of the paris agreement. *Nuclear Engineering and Technology*, page 103350.

[Araya et al., 2020] Araya, S. S., Liso, V., Cui, X., Li, N., Zhu, J., Sahlin, S. L., Jensena, S. H., Nielsen, M. P., and Kær, S. K. (2020). A review of the methanol economy: The fuel cell route. *energies*.

[Busch et al., 2023] Busch, S., Kasdorp, R., Koolen, D., Mercier, A., and Spooner, M. (2023). The development of renewable energy in the electricity market.

[Buttler et al., 2015] Buttler, A., Koltun, R., Wolf, R., and Spliethoff, H. (2015). A detailed techno-economic analysis of heat integration in high temperature electrolysis for efficient hydrogen production. *International Journal of Hydrogen Energy*, 40(1):38–50.

[Cai et al., 2010] Cai, Q., Luna-Ortiz, E., Adjiman, C., and Brandon, N. (2010). The effects of operating conditions on the performance of a solid oxide steam electrolyser: A model-based study. *Fuel Cells*, 10:1114 – 1128.

[Elcogen, 2025] Elcogen (2025). Solid oxide fuel cells. Accessed: 2025-03-11.

[EuropeanCommission, 2021] EuropeanCommission (2021). Fit for 55: Delivering the eu's 2030 climate target on the way to climate neutrality.

[Funke, 2013] Funke, K. (2013). Solid state ionics: from michael faraday to green energy—the european dimension. *Science and Technology of Advanced Materials*, 14(4):043502.

[Hauck et al., 2017] Hauck, M., Herrmann, S., and Spliethoff, H. (2017). Simulation of a reversible sofc with aspen plus. *International Journal of Hydrogen Energy*, 42(15):10329–10340.

[Huo et al., 2021] Huo, H., Xu, K., Cui, L., Zhang, H., Xu, J., and Kuang, X. (2021). Temperature gradient control of the solid oxide fuel cell under variable load. *ACS Omega*, 6(42):27610–27619.

[International Energy Agency, 2024] International Energy Agency, I. (2024). Clean energy is boosting economic growth.

[Laguna-Bercero, 2023] Laguna-Bercero, M. A. (2023). *High Temperature Electrolysis*, volume 95 of *Lecture Notes in Energy*. Springer.

[Lay-Grindler et al., 2013] Lay-Grindler, E., Laurencin, J., Delette, G., Aicart, J., Petitjean, M., and Dessemond, L. (2013). Micro modelling of solid oxide electrolysis cell: From performance to durability. *International Journal of Hydrogen Energy*, 38(17):6917–6929.

[Lienhard and Lienhard, 2024] Lienhard, V, J. H. and Lienhard, IV, J. H. (2024). *A Heat Transfer Textbook*. Phlogiston Press, Cambridge, MA, 6th edition. Version 6.00.

[Menon et al., 2014] Menon, V., Janardhanan, V. M., and Deutschmann, O. (2014). A mathematical model to analyze solid oxide electrolyzer cells (soecs) for hydrogen production. *Chemical Engineering Science*, 110:83–93. Mackie-2013 "Pushing the boundaries".

[Mohebali Nejadian et al., 2023] Mohebali Nejadian, M., Ahmadi, P., and Houshfar, E. (2023). Comparative optimization study of three novel integrated hydrogen production systems with soec, pem, and alkaline electrolyzer. *Fuel*, 336:126835.

[Ni et al., 2007] Ni, M., Leung, M. K., and Leung, D. Y. (2007). Parametric study of solid oxide steam electrolyzer for hydrogen production. *International Journal of Hydrogen Energy*, 32(13):2305–2313. ICHS-2005.

[O'Hayre et al., 2016] O'Hayre, R., Cha, S.-W., Colella, W., and Prinz, F. B. (2016). *Fuel Cell Fundamentals*. 3 edition.

[Perna et al., 2018] Perna, A., Minutillo, M., and Jannelli, E. (2018). Designing and analyzing an electric energy storage system based on reversible solid oxide cells. *Energy Conversion and Management*, 159:381–395.

[Petipas et al., 2013] Petipas, F., Brisse, A., and Bouallou, C. (2013). Model-based behaviour of a high temperature electrolyser system operated at various loads. *Journal of Power Sources*, 239:584–595.

[Rathee, 2023] Rathee, D. (2023). Types of electrolysers: Cef explains.

[Sitte and Merkle, 2023] Sitte, W. and Merkle, R., editors (2023). *High-Temperature Electrolysis*. 2053-2563. IOP Publishing.

[Smolinka and Garche, 2022] Smolinka, T. and Garche, J. (2022). *Electrochemical Power Sources: Fundamentals, Systems, and Applications*. Elsevier.

[Udagawa et al., 2007] Udagawa, J., Aguiar, P., and Brandon, N. (2007). Hydrogen production through steam electrolysis: Model-based steady state performance of a cathode-supported intermediate temperature solid oxide electrolysis cell. *Journal of Power Sources*, 166(1):127–136.

[Wang et al., 2020] Wang, C., Chen, M., Liu, M., and Yan, J. (2020). Dynamic modeling and parameter analysis study on reversible solid oxide cells during mode switching transient processes. *Applied Energy*, 263:114601.

[Wu et al., 2024] Wu, C., Zhu, Q., Dou, B., Fu, Z., Wang, J., and Mao, S. (2024). Thermodynamic analysis of a solid oxide electrolysis cell system in thermoneutral mode integrated with industrial waste heat for hydrogen production. *Energy*, 301:131678.

[Zhang et al., 2020] Zhang, L., Zhao, H., Wilkinson, D., Sun, X., and Zhang, J. (2020). *Electrochemical Water Electrolysis: Fundamentals and Technologies*. Electrochemical Energy Storage and Conversion. CRC Press.

[Zhang et al., 2025] Zhang, R., Jiang, P., and Zhu, Y. (2025). Control-oriented modeling and dynamic behavior analysis of a solid oxide electrolysis cell hydrogen production system. *Fuel*, 390:134648.

Appendix A

Additional SOEC dynamic study

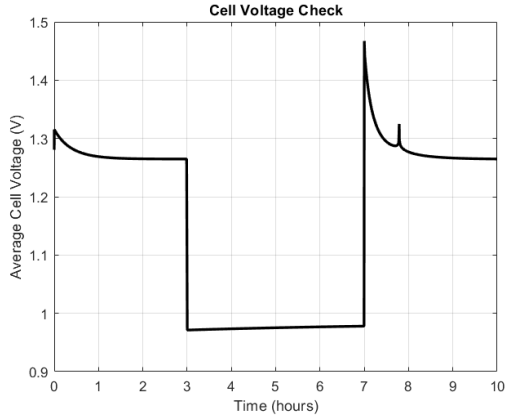

(a) Average Cell Voltage over time.

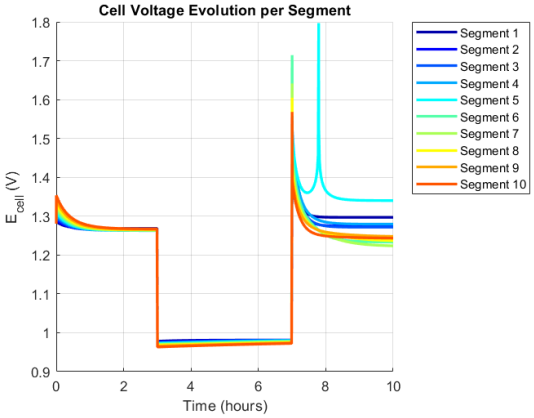

(b) Segment Voltage over time.

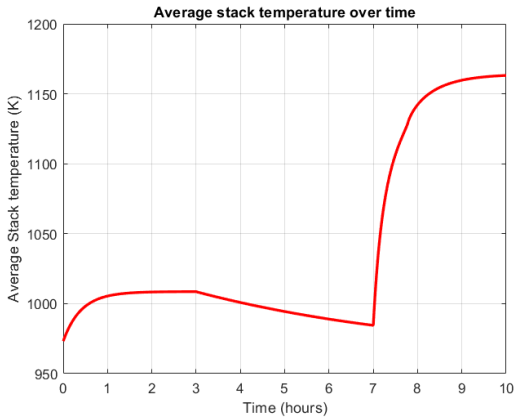

(c) Average Stack Temperature profile over time.

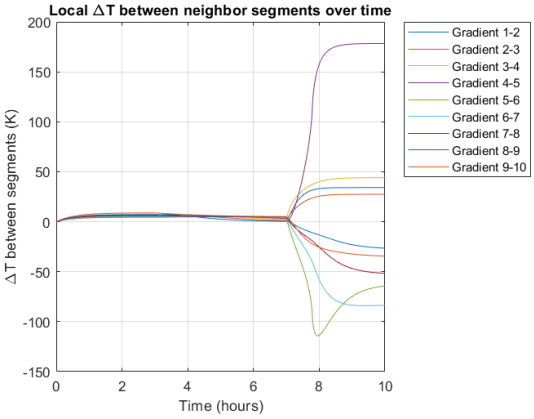

(d) Temperature gradient between segments over time.

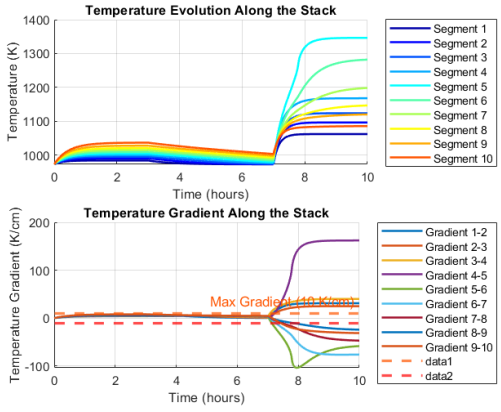

(e) Temperature gradient over time.

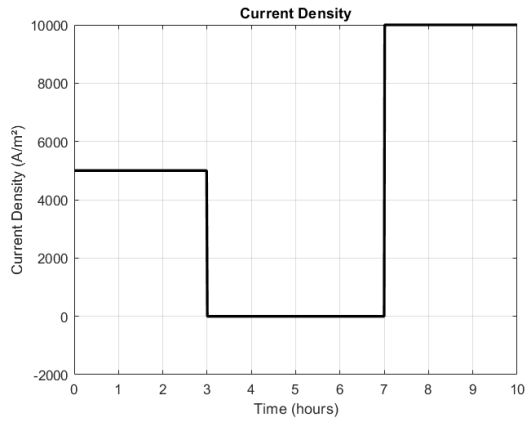

(f) Current density profile over time.

Figure A.1: Dynamic behaviour of the SOEC system under extreme conditions.

In order to have a deeper understanding of the SOEC stack behaviour, another study is performed. Instead of the conditions described in Section 4.2, a current input of 100% and 200% is applied for this purpose.

Figure A.1 illustrates the behaviour of the SOEC stack under extreme operating conditions. The simulation spans a total duration of 10 hours, during which the system is subjected to 100% of the nominal current for the first 3 hours, followed by a 4-hour period with zero current input, and concluding with 3 hours at 200% of the nominal current. It is clear that if the system does not consider heat dissipation, the stack experiences overheating and exceeds the critical temperature gradient limit of 10 K/cm under extreme operating conditions. Mass transport limitations become more pronounced, as shown in Figures A.1b and A.1d, where the temperature distribution becomes increasingly irregular, leading to unstable and potentially unsafe SOEC stack operation. This supplementary simulation highlights the critical importance of implementing effective temperature control strategies and carefully defined operating conditions.

Appendix B

SOEC Dynamic behaviour under constant voltage

In real-world applications, the current profile varies along the stack due to both electronic and ionic resistances. Instead, the voltage remains constant, while the current density fluctuates locally depending on thermodynamic and kinetic conditions. Modelling this behaviour accurately becomes complex, as the voltage input is inherently dependent on various overpotentials, which themselves vary spatially and temporally. The figures below provide insight into stack behaviour under these more realistic operating conditions.

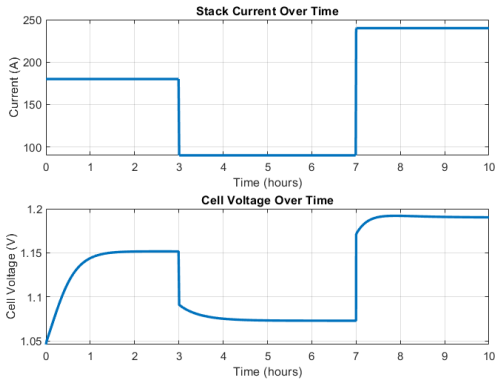

(a) Cell Voltage over time.

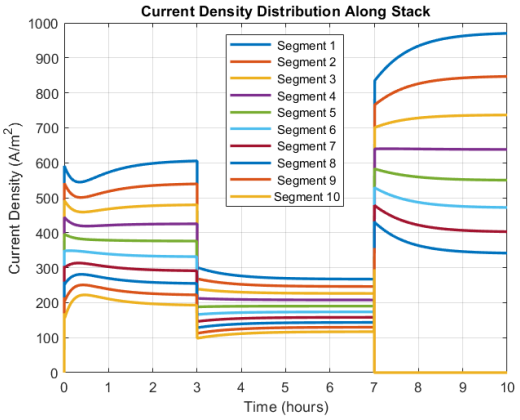

(b) Current density distribution over time.

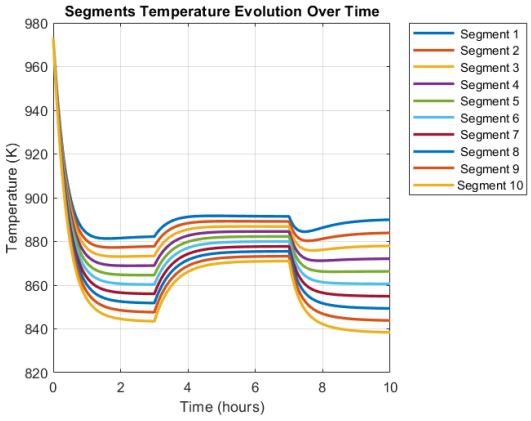

(c) Segments Temperature profile over time.

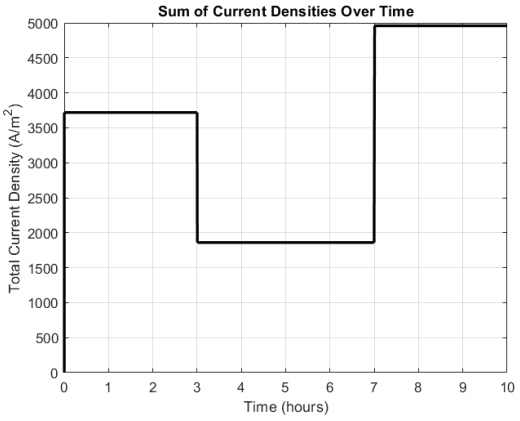

(d) Current Density sum.

Figure B.1: Dynamic behaviour of the SOEC system under constant voltage over the cell length.

Figure B.1 illustrates several parameters of the SOEC stack assuming constant voltage across the segments while allowing for local variations in current density. It can be seen that the energy balance differs substantially from the transient study previously discussed in terms of temperature evolution. In this case, the stack temperature exhibits a more

pronounced decrease during operation, and an unexpected rise during the second load change, where a further decrease would be anticipated. Despite these discrepancies, these results give an overview of how the system operates close to real-world applications.